Please cite this article in press as: Hasan et al., A Fear Memory Engram and Its Plasticity in the Hypothalamic Oxytocin System, Neuron (2019), https://doi.org/10.1016/j.neuron.2019.04.029

Neuron
Article

A Fear Memory Engram and Its Plasticity in the Hypothalamic Oxytocin System

Mazahir T. Hasan,[1,2,3,4,14,15,*] Ferdinand Althammer,[5,14] Miriam Silva da Gouveia,[5,14] Stephanie Goyon,[6,14] Marina Eliava,[5] Arthur Lefevre,[5] Damien Kerspern,[6] Jonas Schimmer,[5] Androniki Raftogianni,[5] Jerome Wahis,[6] H. Sophie Knobloch-Bollmann,[5,16] Yan Tang,[5] Xinying Liu,[5] Apar Jain,[5] Virginie Chavant,[6] Yannick Goumon,[6] Jan-Marek Weislogel,[7,17] René Hurlemann,[8] Sabine C. Herpertz,[9] Claudia Pitzer,[10] Pascal Darbon,[6] Godwin K. Dogbevia,[4,18] Ilaria Bertocchi,[4,11,19] Matthew E. Larkum,[3] Rolf Sprengel,[4,11] Hilmar Bading,[7] Alexandre Charlet,[6,12,15,*] and Valery Grinevich[5,13,15,20,*]

[1]Laboratory of Memory Circuits, Achucarro Basque Center for Neuroscience, Science Park of the UPV/EHU, Sede Building, Barrio Sarriena, 48940 Leioa, Spain
[2]Ikerbasque–Basque Foundation for Science, 48013 Bilbao, Spain
[3]Neurocure, Charité-Universitätsmedizin, Virchowweg 6, 10117 Berlin, Germany
[4]Max Planck Institute for Medical Research, Jahnstrasse 29, 69120 Heidelberg, Germany
[5]Schaller Research Group on Neuropeptides, German Cancer Research Center, Im Neuenheimer Feld 307, 69120 Heidelberg, Germany
[6]Centre National de la Recherche Scientifique and University of Strasbourg, Institute of Cellular and Integrative Neurosciences, 8 Allée du Général Rouvillois, 67000 Strasbourg, France
[7]Department of Neurobiology, Heidelberg University, Im Neuenheimer Feld 364, 69120 Heidelberg, Germany
[8]Department of Psychiatry and Division of Medical Psychology, University of Bonn Medical Center, Sigmund-Freud-Strasse 25, 53105 Bonn, Germany
[9]Department of General Psychiatry, Center of Psychosocial Medicine, Heidelberg University, Voßstraße 4, 69115 Heidelberg, Germany
[10]Interdisciplinary Neurobehavioral Core (INBC), Heidelberg University, Im Neuenheimer Feld 515, 69120 Heidelberg, Germany
[11]Max Planck Research Group at the Institute for Anatomy and Cell Biology, Heidelberg University, Im Neuenheimer Feld 307, 69120 Heidelberg, Germany
[12]University of Strasbourg Institute for Advanced Study (USIAS), Strasbourg, France
[13]Department of Neuropeptide Research for Psychiatry, Central Institute of Mental Health, Heidelberg University, J5, 68159 Mannheim, Germany
[14]These authors contributed equally
[15]Senior author
[16]Present address: Institute of Physiology, University of Freiburg, Hermann-Herder-Strasse 7, 79104 Freiburg, Germany
[17]Present address: BioNTech AG, An der Goldgrube 12, 55131 Mainz, Germany
[18]Present address: Division of Cardiac Surgery, University of Ottawa Heart Institute, Ottawa, ON K1Y 4W7, Canada
[19]Present address: Neuroscience Institute Cavalieri-Ottolenghi, University of Turin, Regione Gonzole 10, 10043 Orbassano, Turin, Italy
[20]Lead Contact
*Correspondence: mazahir.t.hasan@gmail.com (M.T.H.), acharlet@unistra.fr (A.C.), v.grinevich@dkfz-heidelberg.de (V.G.)
https://doi.org/10.1016/j.neuron.2019.04.029

SUMMARY

Oxytocin (OT) release by axonal terminals onto the central nucleus of the amygdala exerts anxiolysis. To investigate which subpopulation of OT neurons contributes to this effect, we developed a novel method: virus-delivered genetic activity-induced tagging of cell ensembles (vGATE). With the vGATE method, we identified and permanently tagged a small subpopulation of OT cells, which, by optogenetic stimulation, strongly attenuated contextual fear-induced freezing, and pharmacogenetic silencing of tagged OT neurons impaired context-specific fear extinction, demonstrating that the tagged OT neurons are sufficient and necessary, respectively, to control contextual fear. Intriguingly, OT cell terminals of fear-experienced rats displayed enhanced glutamate release in the amygdala. Furthermore, rats exposed to another round of fear conditioning displayed 5-fold more activated magnocellular OT neurons in a novel environment than a familiar one, possibly for a generalized fear response. Thus, our results provide first evidence that hypothalamic OT neurons represent a fear memory engram.

INTRODUCTION

Emotional memory representations (also called memory engrams), such as for fear, are pivotal for animal survival. Fear-associated behaviors have evolved over millions of years in living systems, from lower to higher animals, so that they can sense, evaluate, respond, and adapt to adequately deal with dangerous situations (Mobbs et al., 2015). Fear-related disorders, such as specific phobias and post-traumatic stress disorder (PTSD), are among the most prevalent human psychiatric conditions and pose debilitating health burdens to affected individuals and immense costs to society (Kessler and Bromet, 2013). Understanding the neural basis of fear learning, expression,

Please cite this article in press as: Hasan et al., A Fear Memory Engram and Its Plasticity in the Hypothalamic Oxytocin System, Neuron (2019), https://doi.org/10.1016/j.neuron.2019.04.029

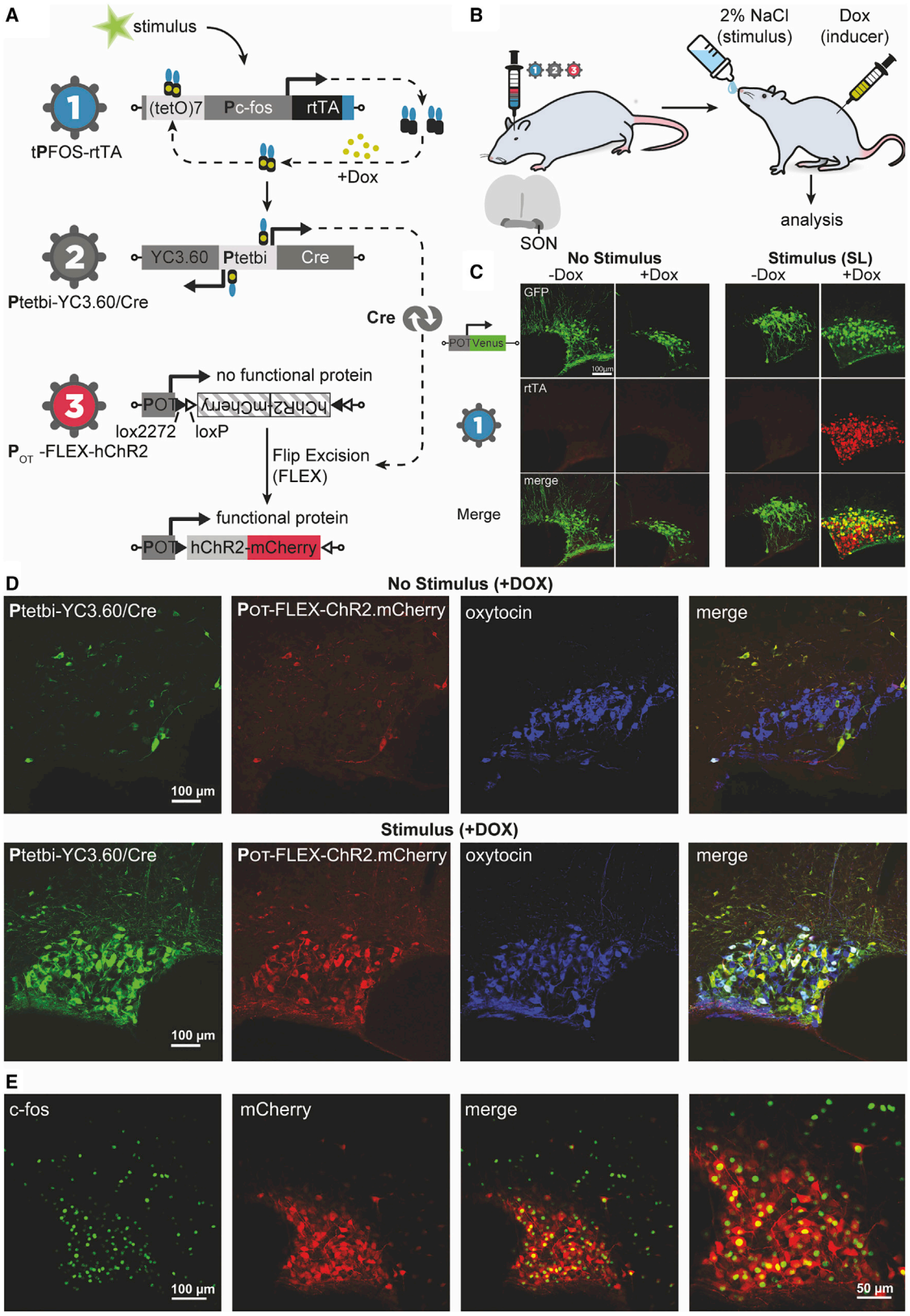

(legend on next page)

and extinction is of paramount importance for PTSD treatment; for example, by targeted circuit-specific therapeutics.

The hypothalamus is an evolutionary old and deeply located brain structure that relays fear-related emotional behavior in mammals. Fear memory engrams are thought to be distributed between the different brain regions in the nervous system; for example, the amygdala, hippocampus, and medial prefrontal cortex (mPFC) (Kitamura et al., 2017). Notably, the hypothalamus is reciprocally connected to different brain regions, including the amygdala (Knobloch et al., 2012) and the mPFC (Heidbreder and Groenewegen, 2003), which, in turn, interact with various other brain regions when organizing fear memories (Tovote et al., 2015). These findings support the view that brain networks, composed of distributed cell assemblies, generate behavior, including the formation of memory representations or engrams. We thus hypothesized that the hypothalamus, being the oldest brain structure, which evolved over time alongside the newer higher brain structures, might be equipped with mechanisms to encode engram-like features and capable of plasticity.

The central nucleus (CeA), a subregion of the amygdala, participates in the acquisition, consolidation, storage, expression, and extinction of fear memories (Ciocchi et al., 2010; Herry et al., 2010; Letzkus et al., 2011) and the subsequent physiological response: freezing behavior (Viviani et al., 2011). Hypothalamic oxytocin (OT) neurons precisely project to the lateral part of the CeA (CeL), where axonal OT release activates CeL neurons (Knobloch et al., 2012), which, in turn, inhibit GABAergic neurons in the medial part of the CeA (CeM), attenuating the fear-related freezing response in rodents. However, the precise role of OT neurons and their projections to the CeA during fear learning is still not well understood. It is unknown which fraction of OT neurons contributes to the anxiolytic effect, how OT neurons are recruited during different fear episodes, and whether the hypothalamus-amygdala circuit is subject to fear-dependent plasticity and contextual specificity.

To tackle these questions, we developed a novel genetic method, virus-delivered genetic activity-induced tagging of cell ensembles (vGATE), to tag fear-experience-activated OT neurons in rats during contextual fear conditioning (FC) (Ehrlich et al., 2009; LeDoux, 2007). Here we provide first evidence that establishes the role of OT neuronal ensembles in fear expression and extinction. We discovered that optogenetic activation of a small subset of fear exposure-activated OT neurons drastically reversed freezing behavior (“unfreezing”) and their silencing impaired context-specific fear extinction. Importantly, fear exposure-tagged OT neurons display an enormous capacity for experience-dependent plasticity by enhancing glutamatergic over OT-ergic transmission in the hypothalamic-amygdalar circuitry. These results clearly demonstrate that fear exposure-tagged OT neurons are both sufficient and necessary for attenuation of fear expression. Altogether, these results satisfy the key criteria of the synaptic plasticity memory hypothesis (Martin et al., 2000) in identifying and validating a fear memory engram in hypothalamic OT circuits. Thus, we conclude that memory engrams are not only restricted to higher brain regions, such as the hippocampus and cortex, but also present in a lower brain region, such as the hypothalamus. This study is a shift in paradigm, revealing the anatomical and functional connectivity organization of fear memory engrams as network-wide distributed cell assemblies that include both higher and lower brain regions.

RESULTS

Activity-Dependent Tagging of OT Neurons

To specifically label activated OT neurons, we developed and describe here a genetic method called vGATE (Figure 1A). In the vGATE system, a c-*fos* promoter ($\mathbf{P}_{fos}$) fragment (Schilling et al., 1991) drives the expression of the reverse tetracycline-sensitive (tet) transactivator (rtTA) (Dogbevia et al., 2015, 2016). In activated neurons, stimulation of the c-*fos* promoter rapidly induces rtTA expression. To obtain sustained rtTA expression for permanent tagging of c-*fos* activated neurons, we designed an autoregulatory expression loop by introducing rtTA-binding DNA sequences (tet operator sequences [$(tetO)_7$]) upstream of $\mathbf{P}_{fos}$ to drive rtTA expression (the full genetic module is $(tetO)_7$-$\mathbf{P}_{fos}$-rtTA). In the presence of doxycycline (Dox), transient $\mathbf{P}_{fos}$ activity drives rtTA expression, which, upon binding to $(tetO)_7$, takes over the transient c-*fos* promoter activity by establishing a Dox-controlled rtTA-dependent and self-sustaining autoregulatory loop (Figure 1A) for persistent rtTA expression. A second virus (virus 2) is equipped with a bidirectional tet promoter ($\mathbf{P}_{tet}$bi) that drives the expression of genes encoding for the Cre recombinase and fluorescent proteins (Figure 1A). Finally, a third virus (virus 3) is equipped with a cell-type-specific promoter (OT in our case) that drives Cre-dependent expression of any gene(s) (Figure 1A).

vGATE-Assisted, Dox-Dependent rtTA Expression *In Vivo*

As a proof of principle, we first validated the vGATE method *in vitro* (Figures S1A–S1D) and, subsequently, *in vivo*. For *in vivo* validation, we injected the vGATE construct rAAV-$(tetO)_7$-$\mathbf{P}_{fos}$-rtTA into the supraoptic nucleus (SON) of the hypothalamus. Three weeks later, rats were treated under four different

Figure 1. Operating Principle of the vGATE System and Activity-Dependent Tagging of OT Neurons

(A) Scheme of the vGATE system: virus 1 (rAAV-$(tetO)_7$-$\mathbf{P}_{fos}$-rtTA), virus 2 (rAAV-$\mathbf{P}_{tet}$bi-Cre/YC3.60), and virus 3 (rAAV-$\mathbf{P}_{OT}$-FLEX-hChR2-mCherry).

(B) Rats were injected with vGATE viral cocktail (3 viruses) into the hypothalamic SON and treated with Dox in combination with osmotic stimulation (salt loading).

(C) Dox-dependent rtTA expression is only detected in the stimulus + Dox group. To verify correct viral targeting of the SON, the rAAV-$(tetO)_7$-$\mathbf{P}_{fos}$-rtTA virus was mixed 1:1 with an rAAV expressing Venus under control of the oxytocin promoter (rAAV-$\mathbf{P}_{OT}$-Venus; Knobloch et al., 2012).

(D) In euhydrated rats (basal, top panel), Dox injection induces rtTA-dependent YC3.60 (via virus 2, green) and Cre-dependent ChR2-mCherry (via virus 3, red) signals in a few scattered neurons. In contrast, both signals were detected in the majority of SON OT neurons (blue) after Dox injection to osmotically challenged, salt-loaded rats (stimulated, bottom panel).

(E) Expression of the endogenous c-*fos* signal (visualized via immunohistochemistry, green) overlays vGATE-assisted the ChR2-mCherry signal (red) in virtually all SON OT neurons of Dox-treated, osmotically challenged rats.

conditions: ± Dox and with or without salt loading (SL), which induced robust c-*fos* expression in OT neurons (Katoh et al., 2010; Figures 1B and 1C; Table S1). Only under the +Dox/+SL condition, robust rtTA expression under a synthetic c-*fos* promoter was detected (red) within 24 h in roughly all of the OT neurons (Hamamura et al., 1991; Figure 1C). This result shows that the vGATE method is compatible with endogenous c-*fos* expression. With rAAV-$\mathbf{P}_{OT}$-Venus as a tracer, it was possible to verify proper virus targeting and spread of infection after injection.

In a different set of experiments, we injected a cocktail of three viruses called OT^{vGATE}: (virus 1, rAAV-$(tetO)_7$-$\mathbf{P}_{fos}$-rtTA; virus 2, rAAV-$\mathbf{P}_{tet}$bi-Cre/YC3.60; virus 3, rAAV-$\mathbf{P}_{OT}$-FLEX-humanized channel rhodopsin (hChR2)-mCherry) and analyzed for YC3.60 (virus 2) and hChR2-mCherry (virus 3). Under +SL/+Dox robust YC3.60 ($\mathbf{P}_{tet}$bi-Cre/YC3.60) and hChR2-mCherry (Cre-dependent, $\mathbf{P}_{OT}$-FLEX-hChR2-mCherry) immunosignals were co-localized in the majority of OT neurons (96.30% ± 1.88% SON, 97.22% ± 2.66% paraventricular nucleus (PVN); Figure 1D). In these animals, we found that 2.4% ± 1.1% (48 of 2,011) of the YC3.60/hChR2-mCherry-expressing cells in the PVN and 5.7% ± 1.4% (132 of 2,320) of cells in the SON were non-OTergic (n = 6 animals). Under the +Dox /−SL (Figure 1D) condition, we found that 7.3% ± 2.2% YC3.60/hChR2-mCherry-positive cells around the SON were non-OTergic (179 of 2,450 neurons) and that 0.8% ± 0.5% YC3.60/hChR2-mCherry-positive cells around the PVN were non-OTergic (22 of 2,450 neurons, n = 6; n = animal number, 6 sections per animal). These unidentified YC3.60/hChR2-mCherry-positive cells were within a radius of 400 μm from the border of the respective nucleus. Under −SL/−Dox conditions (Figure S1E), we observed virtually no YC3.60 and mCherry labeling (0.1% ± 0.03%, 5 of 540 for the PVN; 0.3% ± 0.09%, 22 of 722 for the SON; n = 6, 6 sections per animal), a result of minimal leakiness of the $\mathbf{P}_{tet}$bi. Furthermore, we observed more than 93% (94.74% ± 1.75% for the SON and 93.56% ± 2.46% for the PVN; Table S1) co-localization of endogenous c-*fos* and mCherry in vGATE animals subjected to SL for 5 consecutive days (Figure 1E).

Optogenetic Stimulation of Tagged OT Neurons Reverses Freezing Behavior in Fear-Conditioned Rats

We investigated what fraction of the entire OT population actually contributes to the anxiolytic effect and how OT neurons are recruited during the expression of fear using contextual FC in rats (Figure 2A). We found that only a small number of OT neurons in the SON and PVN expressed c-*fos* during fear exposure (Figures S2A and S2B). Next we generated OT^{vGATE} rats with bilateral injections of the vGATE viral cocktail to permanently tag activated OT neurons in the SON and PVN for activity manipulation by hChR2 (virus 1, rAAV-$(tetO)_7$-$\mathbf{P}_{fos}$-rtTA; virus 2, rAAV-$\mathbf{P}_{tet}$bi-Cre/YC3.60; virus 3, rAAV-$\mathbf{P}_{OT}$-FLEX-hChR2-mCherry) (OT^{vGATE}). We specifically chose day 3 for the Dox injection because we wanted to exclusively label fear-activated OT neurons but not pain-sensitive OT neurons. As a control, we generated rats that constitutively expressed rAAV-delivered hChR2 in all OT neurons ($OT^{Constitutive}$) in the SON and PVN. Although the $OT^{Constitutive}$ group displayed viral expression in virtually all OT neurons (99.4% ± 0.8%, n = 4; Figure 2B1), in the OT^{vGATE} group, only a small fraction of the OT neurons was tagged during fear expression (341 of 2,470, 13.8% ± 0.7% of OT neurons in the SON and 331 of 2,666, 12.4% ± 1.6% of OT neurons in the PVN) of ~6,600 cells comprising the PVN and SON in rats (Althammer and Grinevich, 2017; Figure 2B2; Table S2). We found that only 1.2% of non-OTergic cells were labeled non-specifically (57 cells of 2,051 cells in total labeled via vGATE, PVN/SON combined, n = 4, 6 sections per animal) in the fear-conditioned animals (Figure S2C). To determine whether OT^{vGATE} neurons project axons terminating within the CeA subregion of the amygdala, we analyzed brain slices containing the CeL and found mCherry-positive fibers in the CeL that were also OT-immuno-positive (Figure 2B2). Optogenetic stimulation of these OT axons in the CeL with blue light (BL) induced a prominent decrease in the freezing response (unfreezing) in both groups. Surprisingly, the BL-evoked unfreezing effect in the OT^{vGATE} group was much stronger (freezing time, 6.9 ± 1.1 s versus 38.1 ± 7.6 s, $p < 0.0001$; Figure 2C2) and occurred faster (onset, 3.8 ± 0.7 s versus 25.9 ± 10.8 s, $p < 0.0001$; Figure 2D) than in the $OT^{Constitutive}$ group (Figures 2C1 and 2D). To rule out that the observed behavioral changes were mediated by brain regions other than the CeA, we injected 4 animals with rAAV-$(tetO)_7$-$\mathbf{P}_{fos}$-rtTA, rAAV-$\mathbf{P}_{tet}$bi-Cre/YC3.60, and rAAV-$\mathbf{P}_{OT}$-FLEX-GFP. Four animals injected with rAAV-$\mathbf{P}_{OT}$-Venus served as a control. We analyzed the brains of the vGATE-injected animals and did not find any GFP-positive fibers outside of the CeA, whereas control animals showed prominent labeling of OT fibers in various brain regions, as reported previously (Figure S2D; Knobloch et al., 2012). This indicates that fear-activated, vGATE-labeled OT neurons project exclusively to the CeA. In addition, we did not find a single mCherry-positive fiber in the CeA that was negative for OT immunoreactivity (n = 6 animals, 6 sections per animal, in which more than 15 mm of total axon length was analyzed), indicating that axonal projections from vGATE-labeled axons exclusively represent OT fibers. Conversely, we found no difference between $OT^{Constitutive}$ (98.2% ± 1.4%, n = 6) and OT^{vGATE} (96.9% ± 2.1%, n = 6) groups regarding the labeling of OT-positive fibers in the CeL, indicating that all OT neurons projecting to the CeL are fear-sensitive. Next, to provide additional proof that OT^{vGATE} neurons precisely project to the CeA, we injected green Retrobeads into the CeA of rats with OT^{vGATE} neurons labeled by mCherry. The anatomical analysis revealed that 94.6% ± 3.1% of mCherry-positive OT neurons (1,337 OT^{vGATE} neurons, PVN/SON combined, n = 4) contained green Retrobeads (Figure S2E), indicating that the vast majority of OT^{vGATE} neurons project to the CeA.

Because our FC paradigm comprised an additional shock session (day 14, memory reinforcement) to achieve higher basal freezing rates, we wanted to rule out the possibility that this session leads to recruitment of new OT cells. Therefore, we performed another experiment in which animals were injected with rAAV-$(tetO)_7$-$\mathbf{P}_{fos}$-rtTA and rAAV-$\mathbf{P}_{tet}$bi-Cre/YC3.60 and subjected to our FC paradigm (day 3 Dox injection, day 4 shock; Figure S2F). On day 14, animals received an injection of rAAV-$\mathbf{P}_{OT}$-FLEX-hChr2-mCherry and were subjected to another round of FC 2 weeks later. Then one group received another Dox injection, and the control group was injected with saline one day prior to the additional shock session on day 29 (Figure S2F). Although

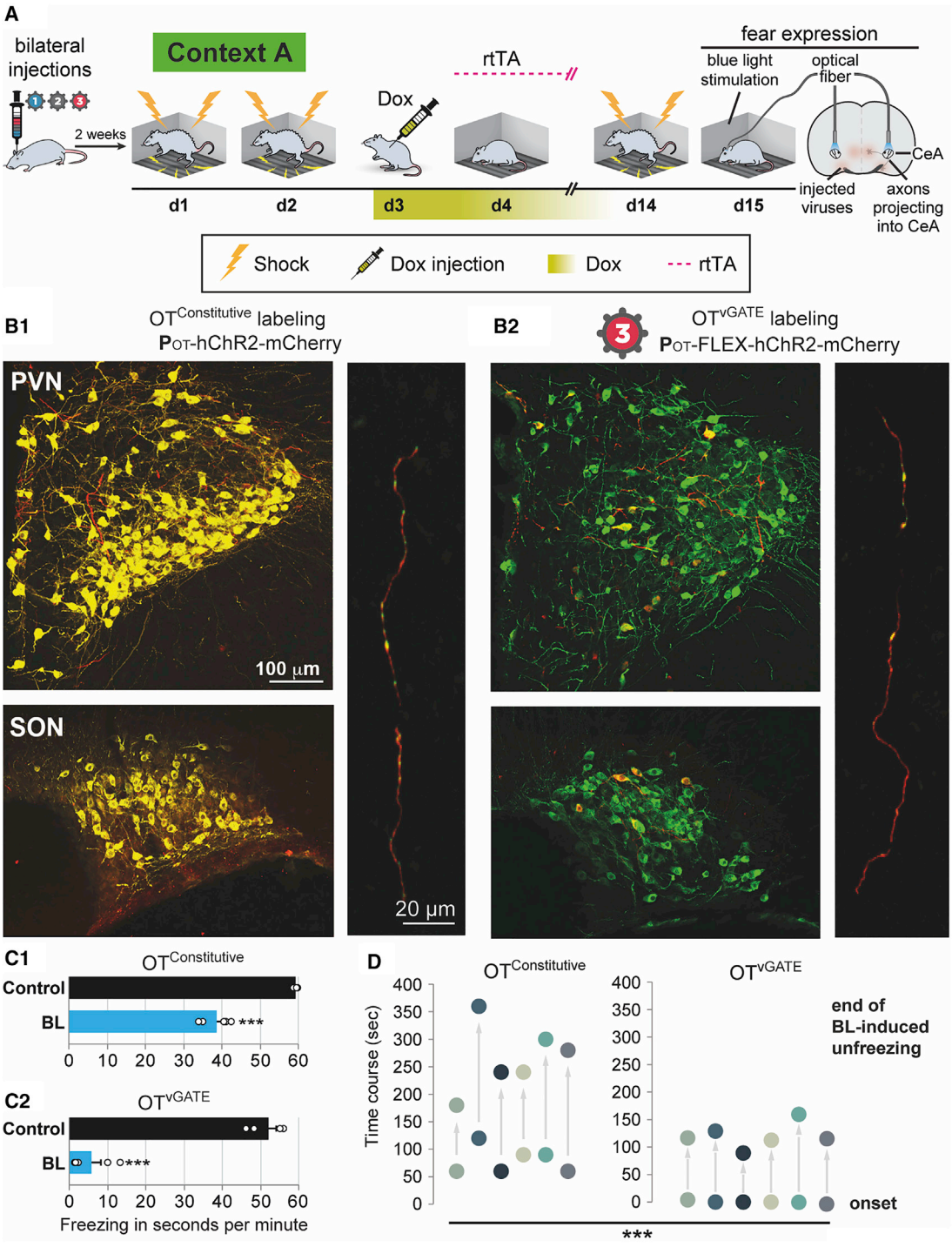

Figure 2. Fear Learning and Optogenetic Control of Fear Behavior

(A) Scheme of the fear condition setup, Dox administration, and blue light stimulation of the CeA.

(B) The vast majority of OT neurons (99.4% ± 0.8%, green) of the PVN and SON were labeled via a constitutive OT promoter driving hChR2-mCherry (B1, red). (B2) Fear expression induced tagging (ChR2-mCherry, red) of a small population of OT neurons (green). (B1 and B2) Vertical panels depict ChR2-mCherry-containing axons (red) with OT-immunopositive puncta (green, appearing in yellow) in the CeL of both groups.

(C) The freezing time before and after blue light illumination of the CeA (C1, top graph: constitutive hChR2 expression, $OT^{Constitutive}$ group; C2, bottom graph: OT^{vGATE} group). The black bars (control) show the freezing time immediately prior to BL stimulation, whereas the blue bars (BL) indicate the freezing time after BL stimulation. ***$p < 0.001$, t test.

(D) The onset and duration of the BL-induced unfreezing effect. Data are presented as mean ± SEM.

the group that was injected with Dox twice displayed normal labeling (224 of 2,033, 11% ± 1.4% for the PVN; 260 of 1,940, 13.4% ± 1.7% for the SON; n = 5; Figure S2G) of OT neurons, we only found a total of 11 mCherry-positive cells in the PVN (11 of 2,020, 0.5%, n = 5) and 17 mCherry-positive cells in the SON (17 of 2,177, 0.8%, n = 5) in the group receiving saline in the first round (Figure S2G). Thus, this experiment demonstrates that, after Dox has been cleared from the brain, only few additional OT cells get labeled. To verify that the comparable labeling of cells also held true on the axonal level, we compared OT-positive fibers within the CeA of animals perfused after 14 days with animals perfused after 43 days (2 weeks after the day 29 shock session; Figure S2F) and found no difference in vGATE-mediated labeling (day 14: 96.9% ± 2.1%, n = 6; day 43: 95.3% ± 3.1%, n = 6).

Because a recent study highlighted the existence of freezing-promoting (somatostatin-ergic) and flight-promoting (corticotropin-releasing hormone-ergic) neurons (Fadok et al., 2017), we sought to find out which cell types within the CeL are activated upon BL stimulation. Therefore, we injected rats with our vGATE viruses (rAAV-$(tetO)_7$-$\mathbf{P}_{fos}$-rtTA and rAAV-$\mathbf{P}_{tet}$bi-Cre/YC3.60) and either rAAV-$\mathbf{P}_{OT}$-FLEX-Venus (n = 4) or rAAV-$\mathbf{P}_{OT}$-FLEX-hChr2-mCherry (n = 4) and subjected them to our FC protocol (Figure 2A). On day 15, we illuminated the CeL for 2 min and sacrificed animals 90 min later. We found that fear exposure itself did not cause c-*fos* expression in the CeL, whereas BL stimulation robustly induced c-*fos* in this structure. In the BL-stimulated animals, we counted 888 corticotropin-releasing hormone (CRH)-positive neurons and 290 SOM-positive neurons, whereas 104 neurons expressed both markers. 84% ± 3.6% of exclusively SOM-positive neurons, 11% ± 0.9% of exclusively CRH-positive neurons, and 58% ± 4.3% of the mixed population expressed c-*fos* (Figure S2H). Thus, these findings suggest that OT release in the CeL predominantly activates SOM-positive interneurons.

Fear-Experience-Dependent Anatomical and Functional Plasticity of Hypothalamic OT Neurons Projecting to the CeA

To investigate potential anatomical and molecular changes following fear experience, we generated OT^{vGATE} rats (virus 3, rAAV-$\mathbf{P}_{OT}$-FLEX-GFP) and quantitatively analyzed OT axons within the CeL. In parallel, we analyzed fear-naive rats expressing $\mathbf{P}_{OT}$-Venus for constitutive labeling of all OT neurons ($OT^{Constitutive}$; Figure 3A1). Although the total length of axonal segments was similar in both groups (Figure 3A3), there was a substantial increase (~3-fold) in the numbers of GFP-positive axonal varicosities containing immunosignals of vesicular glutamate transporter 2 (vGluT2) in the OT^{vGATE} group (Figure 3A3; Table S3). Furthermore, we found that the detectable OT levels in vGATE fibers were at least 3-fold lower compared with the fear-naive animals injected with $\mathbf{P}_{OT}$-Venus, potentially resulting from the enhanced glutamate expression (fear-naïve, 58.0% ± 8.4%; fear-experienced, 15.3% ± 3.1%; signal intensity, n = 4; 6 sections per animal; Figure S3A).

To elucidate the seemingly counter-intuitive observation that activation of a small subset of OT neurons resulted in a stronger behavioral response than activation of axons originating from virtually all OT neurons ($OT^{Constitutive}$ group) in the CeL, we next aimed to investigate the underlying circuitry within the CeA by *ex vivo* electrophysiology in acute brain slices from fear-naive $OT^{Constitutive}$ and fear-experienced OT^{vGATE} groups (Figure 2D). In the naive group, all OT neurons constitutively expressed hChR2 ($OT^{Constitutive}$), whereas in the OT^{vGATE} group, a small fraction of OT neurons was labeled with the vGATE virus cocktail (virus 3, $\mathbf{P}_{OT}$-FLEX-hChr2-mCherry). In both groups, BL stimulation of OT axons in the CeL (Figure 3B) induced an increase in inhibitory postsynaptic current (IPSC) frequencies in neurons of the CeM, which receive direct synaptic input from GABAergic neurons of the CeL (Figure 3C1). Interestingly, the BL-induced increase in CeM IPSC frequencies in the OT^{vGATE} group was almost entirely blocked by the glutamate AMPA receptor antagonist NBQX, whereas it only had a minor effect on the control group (Figure 3C2). On the other hand, the application of the OT receptor antagonist dOVT diminished the BL-induced increase in CeM IPSCs in the OT^{vGATE} group by only 50%, whereas it prevented the increase in CeM IPSCs in the control $OT^{Constitutive}$ group entirely (Figure 3C2).

To rule out that the observed differences were not a result of the fear experience, we injected an additional group of animals with rAAV-$\mathbf{P}_{OT}$-hChR2-mCherry ($OT^{Constitutive}$) and subjected them to the same paradigm as the OT^{vGATE} group (Figure 2A; Figure S3B1). Analysis of the fear-conditioned $OT^{Constitutive}$ group revealed that the BL-induced unfreezing effect, onset, and duration of mobility time (Figures S3B2–S3B4) as well as the effects of NBQX and dOVT on IPSC frequencies in CeM neurons (Figures S3B5–S3B7) were comparable with those observed in the OT^{vGATE} group (Figures 2C, 2D, 3C1, and 3C2). These findings suggest that the initial exposure to FC induced plastic changes in OT neurons, resulting in prevalent release of glutamate from their axonal terminals within the CeL. Because of the similarity of behavioral and amygdala responses to OT axon stimulation in fear-experienced $OT^{Constitutive}$ and OT^{vGATE} groups, the observed effects might stem from the same population of OT neurons naturally activated in both groups of rats during fear expression (Figure 2B).

To test whether the *ex vivo* findings have a functional relevance *in vivo*, we blocked the OT receptor specifically with an antagonist (OTA, L-368,899, 1 mg/kg intraperitoneally [i.p.]) that crosses the blood-brain barrier (Eliava et al., 2016). First, we injected rats bilaterally in the SON and PVN with $\mathbf{P}_{OT}$-hChR2-mCherry ($OT^{Constitutive}$) for optogenetic tagging and implanted optic fibers into the CeA (Figure 3D1). Next we subjected the animals to the FC paradigm. On day 3, treatment of the animals with OTA 40 min prior to BL stimulation (session 1, OTA + BL1) completely prevented the BL-induced unfreezing effect (Figure 3D2). However, 2 weeks later, when we exposed the very same animals to the second session of FC (session 2, OTA + BL2), the animals displayed a rapid BL-induced unfreezing response despite prior application of OTA (Figure 3D3). Interestingly, the onset of BL-induced unfreezing occurred much faster (6 ± 0.8 s versus 25.9 ± 10.8 s, $p < 0.0001$; Figure 3D4) than in the fear-naive $OT^{Constitutive}$ group (Figure 2D). To exclude that the observed unfreezing effects were a result of OTA-induced changes in plasticity originating from the first round of FC, we processed an additional group of animals constitutively

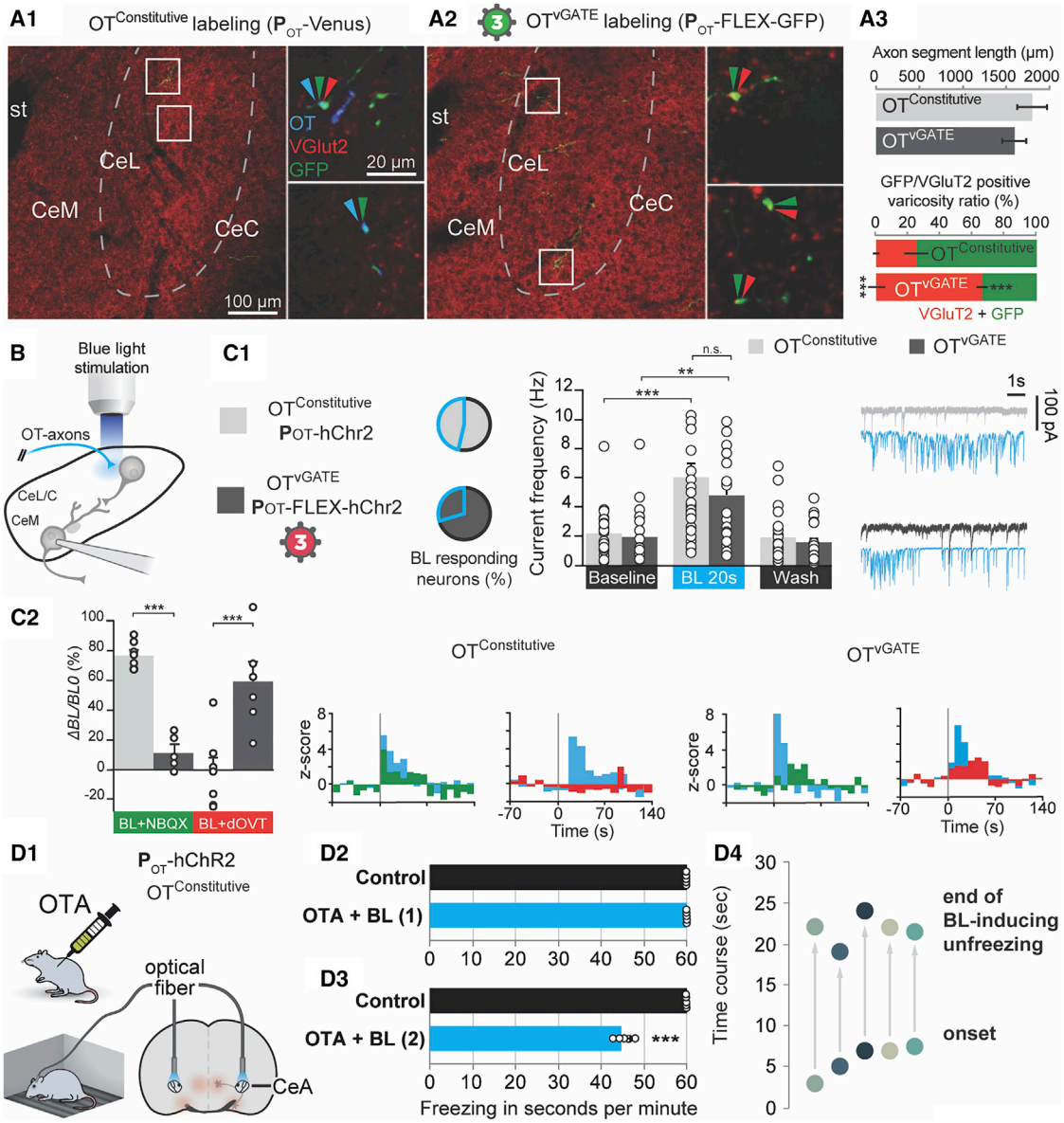

Figure 3. Functional Plasticity of the OT System upon Fear Learning

(A) GFP-labeled axons of OT neurons in the CeL of naive OT^{Constitutive} (A1) and OT^{vGATE} (A2) rats. Shown are an overview and enlarged fragments, showing co-localization of GFP (green) with OT (blue) and vGluT2 (red). (A3) Quantification of total axonal lengths and vGluT2-immunoreactive puncta. Green, OT axons containing no vGluT2; yellow, co-localization of OT and vGluT2; st, *stria terminalis*. *p < 0.05, ***p < 0.001, t test.

(B) Scheme of the *ex vivo* recording setup.

(C) Effect of optical stimulation of OT-ergic axons present in the CeL (BL) on IPSC frequencies recorded in CeM neurons in both fear-naive and fear-experienced vGATE animals (C1). Pie charts depict the proportion of CeM neurons responding to BL (naive OT^{Constitutive}, n = 27 of 56; OT^{vGATE}, n = 23 of 78, not significant).The bar plot shows the change in CeM current frequencies (hertz) in response to BL. Data are expressed as means across slices plus SEM. Individual values are indicated as white circles. **p < 0.01, ***p < 0.001, two-way ANOVA followed by Sidak *post hoc* test. (C2) Pharmacological dissection of BL effects. Left: quantification of the effect of NBQX (green; naive OT^{Constitutive}, n = 7; OT^{vGATE}, n = 5) or dOVT (red; OT^{Constitutive}, n = 7; OT^{vGATE}, n = 6) application on the initial BL effect on IPSC frequencies recorded in the same CeM neurons. Data are expressed as means across slices plus SEM. Individual values are indicated as white circles. ***p < 0.001, Mann-Whitney test. Right: *Z* scores illustrating the time course and modulation of BL effects by NBQX or dOVT.

(D) Scheme of BL stimulation of the CeL in OT^{Consitutive} animals pretreated with OTA (D1). (D2 and D3) The bar charts display the freezing time in the corresponding group and after blue light stimulation of the CeA after OTA administration. Top graph: the first conditioning session (D2, OTA-BL1). Bottom graph: the second conditioning session (D3, OTA-BL2). The black bars (control) show the freezing time immediately prior to BL stimulation, whereas the blue bars (BL) indicate the freezing time after BL stimulation. ***p < 0.001, t test. (D4) Graph displaying the onset and duration of the BL-induced unfreezing effect.

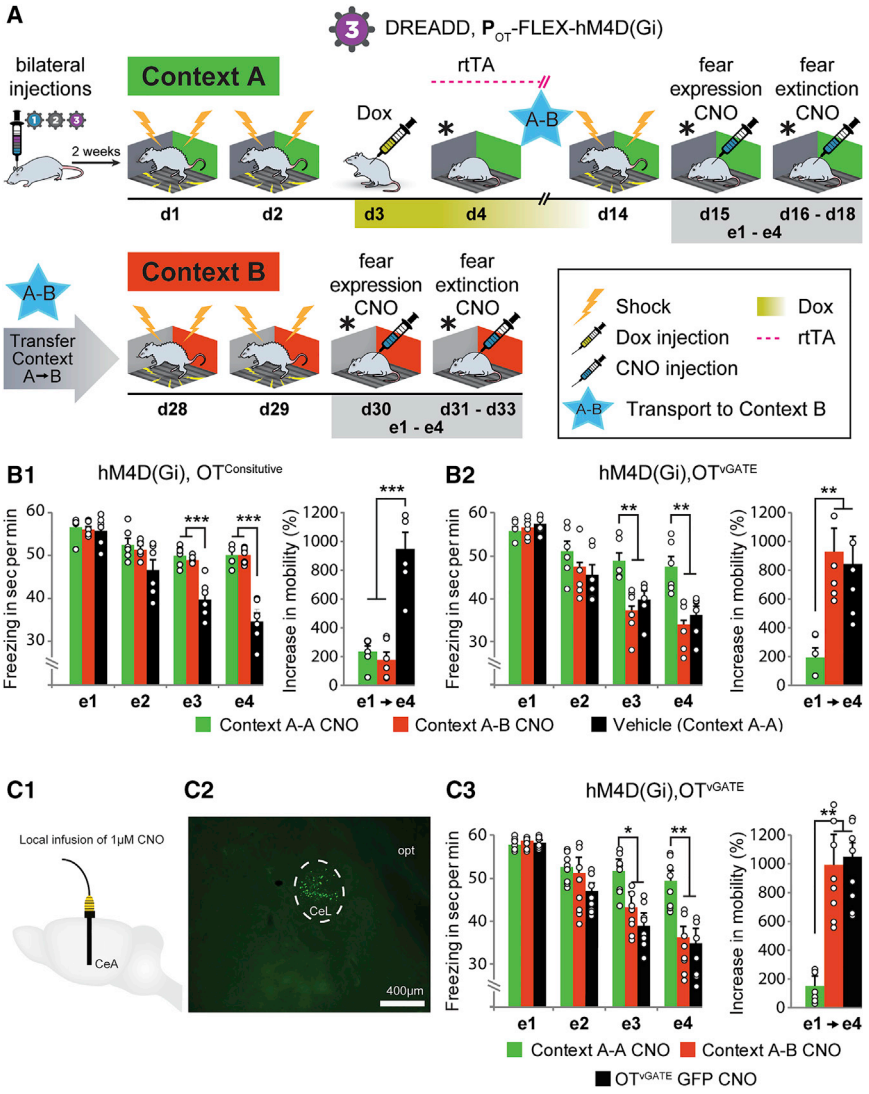

Figure 4. Pharmacogenetic Inhibition of OT Neurons Impairs Fear Extinction

(A) Scheme of the FC setup in contexts A and B (context A, green wall; context B, red wall). Virally injected animals were subjected to contextual FC. After two shock sessions (day 1 and day 2), animals received an i.p. injection of Dox on day 3, followed by another session on day 4 without shocks. Ten days later, animals were subjected to an additional shock day to reinforce the fear memory and then underwent a 4-day fear extinction protocol. During the extinction session, animals received a daily injection of CNO 40 min prior to the experiment. After exposure to context B, animals were subjected to 2 days of shock, followed by another 4-day extinction session, where they again received CNO daily prior to the experiment.

(B) Bar charts showing the average freezing time of animals over the course of a 4-day fear extinction paradigm as well as the total increase in mobility; e1–e4 indicate extinction days. (B1) Although control animals underwent normal fear extinction, CNO-mediated silencing of all OT neurons equally impaired fear extinction in both contexts. $^{**}p < 0.01$, $^{***}p < 0.0001$, t test. (B2) CNO-mediated silencing of vGATE-tagged OT neurons in context A impaired fear extinction in context A but not in context B. $^{**}p < 0.01$, $^{***}p < 0.0001$, one-way ANOVA.

(C) Schematic depiction of the local CNO infusion onto the CeA (C1). (C2) Confocal image showing the site-specific infusion of Retrobeads following CNO infusion to verify proper targeting of the CeA. (C3) Local infusion of CNO into the CeA impaired fear extinction in context A but not context B. $^{*}p < 0.05$, $^{**}p < 0.01$.

expressing hChR2 in OT neurons, which received saline (instead of OTA) in the first session and OTA in the second session, and obtained similar results (Figures S3C1–S3C3) as in the initial group, which was treated with OTA in both sessions (Figure 3D). Thus, our data indicate that fear experience drives a shift from OT to glutamate release from OT axons in the CeL of fear-experienced groups. Moreover, the enhanced responsiveness of CeL neurons to glutamate and its correlated effect, which could be abolished by application of NBQX (Figure 3C2), may indicate a transient, fear-experience-induced upregulation of AMPA receptors in these cells.

Inhibition of Fear-Activated OT Neurons Impairs Fear Extinction in a Context-Dependent Manner

To provide further evidence that OT neurons activated by fear exposure attenuate fear expression, we hypothesized that silencing of OT^{vGATE} neurons inhibits fear extinction specifically in the context where these neurons had originally been activated. Therefore, rats (n = 6) were injected with a virus expressing the modified human muscarinic receptor hM4D(Gi) under control of the OT promoter exposed to contextual FC and extinction paradigms (Figure 4A). All four groups of animals (OT^{vGATE} A-A, OT^{vGATE} A-B, OT^{Constitutive} A-A, and OT^{Constitutive} A-B) were subjected to FC in context A (day 1 shock, day 2 shock, day 3 Dox injection, day 4 exposure). To induce fear extinction, the two groups (OT^{vGATE} A-A and OT^{Constitutive} A-A) were exposed to the same context A for four consecutive days (40 min each session) without any electrical shock, receiving a daily i.p. injection of clozapine-N-oxide (CNO) 40 min prior to testing (control groups received saline). In parallel, we processed two additional groups of animals (OT^{vGATE} A-B and OT^{Constitutive} A-B, n = 6) in analogy to the first groups that were submitted to a first round of FC (in context A) and then transferred to a novel context (context B; Figure 4, blue star) prior to being submitted to the extinction protocol. We introduced the novel context (context B) to specifically investigate the potential role of OT in context-dependent fear extinction. This context represented a novel environment that was distinct in terms of visual, tactile, and olfactory cues (Figure S4A). Importantly, rats conditioned in context A did not display contextual FC in context B (Figure S4B), clearly demonstrating that

animals are able to discriminate between the two boxes (the complete dataset on freezing behavior is provided in Table S4). Silencing of all OT neurons by constitutively expressed hM4D(Gi) and application of its agonist CNO resulted in impaired fear extinction in both contexts A and B (Figure 4B1; Table S4). We next applied the vGATE technique to express hM4D(Gi) specifically in OT neurons (virus 3, rAAV-$\mathbf{P}_{OT}$-hM4D-Gi). We discovered that the silencing of OT fear neurons that were tagged in context A impaired fear extinction in context A but not in the novel context B (Figure 4B2). Because CNO has been reported to potentially activate certain neurons (Gomez et al., 2017), we performed control experiments (without virus injection, n = 6), where CNO alone had no effect on context-specific fear extinction (Figure S4C). To further rule out that the observed differences in fear extinction dynamics were a result of the two different contexts, we subjected naive, non-injected animals to fear extinction sessions in both contexts and found comparable freezing times throughout the extinction sessions (n = 6; Figure S4D).

To demonstrate that the observed impairments in fear extinction stem from inhibition of local OT release onto the CeA, we injected rats (n = 8) with the vGATE cocktail (virus 3, rAAV-$\mathbf{P}_{OT}$-hM4D-Gi) and implanted bilateral guide cannulas above the CeA for local infusion of CNO (Figures 4C1–4C2). CeA local infusion of 1 μM CNO (Stachniak et al., 2014) 15 min prior to each session impaired fear extinction in context A but not context B (Figure 4C3), confirming our previous results. To verify proper targeting of the CeA, we infused Retrobeads immediately after the last extinction session and killed the animals 10 min later to avoid spreading of the tracer (Figure 4C2). The control group (n = 8) injected with vGATE-GFP viruses displayed normal fear extinction in both contexts, indicating that local infusion of CNO per se does not impair fear extinction (Figure 4C3).

Activity of OT Neurons in the SON Is Context Dependent

To shed light on the cellular mechanisms underlying the context-dependent effect of neuronal inhibition (Figure 4B2), we labeled the OT^{vGATE} neurons green with the rAAV-$\mathbf{P}_{OT}$-FLEX-GFP (virus 3) and co-stained sections for endogenous c-*fos* red to identify the fraction of OT cells that was active during re-exposure to the same context (Figure 5A). In line with previous results (Figure 2B2), the first round of context A FC induced tagging of 10.8% of OT neurons in the PVN and 11.9% in the SON, visualized by intrinsic GFP (Figure 5A). The second round of context A FC induced c-*fos* signal in 9.5% of OT neurons in the PVN and 16.2% in the SON (Figure 5A). The overlap of virally expressed GFP and c-*fos* was 18% in the PVN and 89% in the SON, suggesting context-dependent activity of OT neurons specifically in the SON as well as a functional difference between the two nuclei. The difference in re-activation of OT cells in context A→A versus context A→B was significant for the SON (context A-A, 89% ± 5.5%; context A-B, 22% ± 3.6%; n = 6, $p < 0.0001$) but not the PVN (context A-A, 18% ± 2.7%; context A-B, 31% ± 3.7%; n = 6, p = 0.2805; Table S5). It is important to note that the group of animals that was first exposed to context A displayed ~5 times more activated neurons in both the PVN and SON after further exposure to context B (PVN: context A vGATE-GFP, 9.6%; context B c-*fos*, 47.1%; SON: context A vGATE-GFP, 11.7%; context B c-*fos*, 56.4%; Figure 5B; Table S5). This 5-fold difference in neuronal OT activity in context B correlated with the dramatically increased OT concentration in the blood (27.64% ± 5.4% pmol/mL versus 86.7% ± 12.9% pmol/mL; Figure S5A). However, despite the massive recruitment of new cells, the overlap of GFP-positive and c-*fos*-expressing OT neurons in the SON in context B amounted to only 22%. Taken together, these results indicate that re-exposure to a familiar FC context reactivates the same fraction of OT neurons, whereas exposure to a novel context recruits an entirely different population of cells. Therefore, it is plausible that OT neurons participate in a long-lasting fear memory engram that coordinates the OT-ergic response to different contextual fear episodes.

Finally, to investigate whether OT engram cells display basic electrophysiological properties distinct from non-engram OT cells, we performed an additional experiment where we injected animals (n = 12) with vGATE (virus 3, $\mathbf{P}_{OT}$-FLEX-GFP) and $\mathbf{P}_{OT}$-mCherryChr2 into the SON only. Animals were fear-conditioned, received an injection of Dox on day 3, and were processed for *ex vivo* patch-clamp recordings. In these animals, non-engram OT cells expressed red fluorescence, whereas vGATE-labeled engram cells appeared in yellow (green + red) (Figure 5C1). We analyzed access resistance, membrane capacitance, membrane potential, spontaneous excitatory postsynaptic current (EPSC) amplitudes and frequencies, and discharge profile upon current steps. Interestingly, we found significant differences in membrane capacitance (OT non-engram: 20.81 ± 1.25 pF, n = 16; OT engram: 26.13 ± 1.52 pF, n = 24; $p < 0.05$; Figure 5C2) and frequency of spontaneous EPSCs (OT non-engram, 1.87 ± 0.51; OT engram, 3.18 ± 0.54 Hz; $p < 0.05$; Figure 5C2). All other parameters did not significantly differ between $OT^{Constitutive}$ and OT^{vGATE} cells (Figure S5B). Thus, these findings suggest that vGATE-labeled OT engram cells have a larger membrane surface and receive more excitatory inputs, a feature of engram cells that has already been described for the hippocampus (Kitamura et al., 2017; Ryan et al., 2015).

To investigate whether increased glutamatergic input onto OT^{vGATE} could potentially underlie the observed differences in membrane capacitance and increased spontaneous EPSCs, we stained brain slices of vGATE-injected rats with the vesicular glutamate transporter vGluT2 and compared the number of vGluT2-positive puncta in the immediate surroundings (surface of soma and 5-μm radius around each OT-positive neuron). We found that the number of vGluT2 puncta encompassing the OT engram (OT^{vGATE}) cells (18.6 ± 1.2, 130 cells, n = 3) was significantly higher ($p < 0.001$) compared with non-engram OT neurons (8.3 ± 0.9, 1,044 cells, n = 3) (Figure 5C3). These results suggest that OT engram cells receive more prominent glutamatergic input than OT non-engram cells, potentially explaining the unique electrophysiological properties of engram OT neurons (Figure 5C2).

Parvocellular OT Neurons Activate Magnocellular OT Neurons in a Novel Context

Because the OT system is composed of two types of neurons, magnocellular (magnOT) and parvocellular (parvOT) neurons (Rhodes et al., 1981; Swanson and Kuypers, 1980; Swanson and Sawchenko, 1983), we next aimed to investigate which

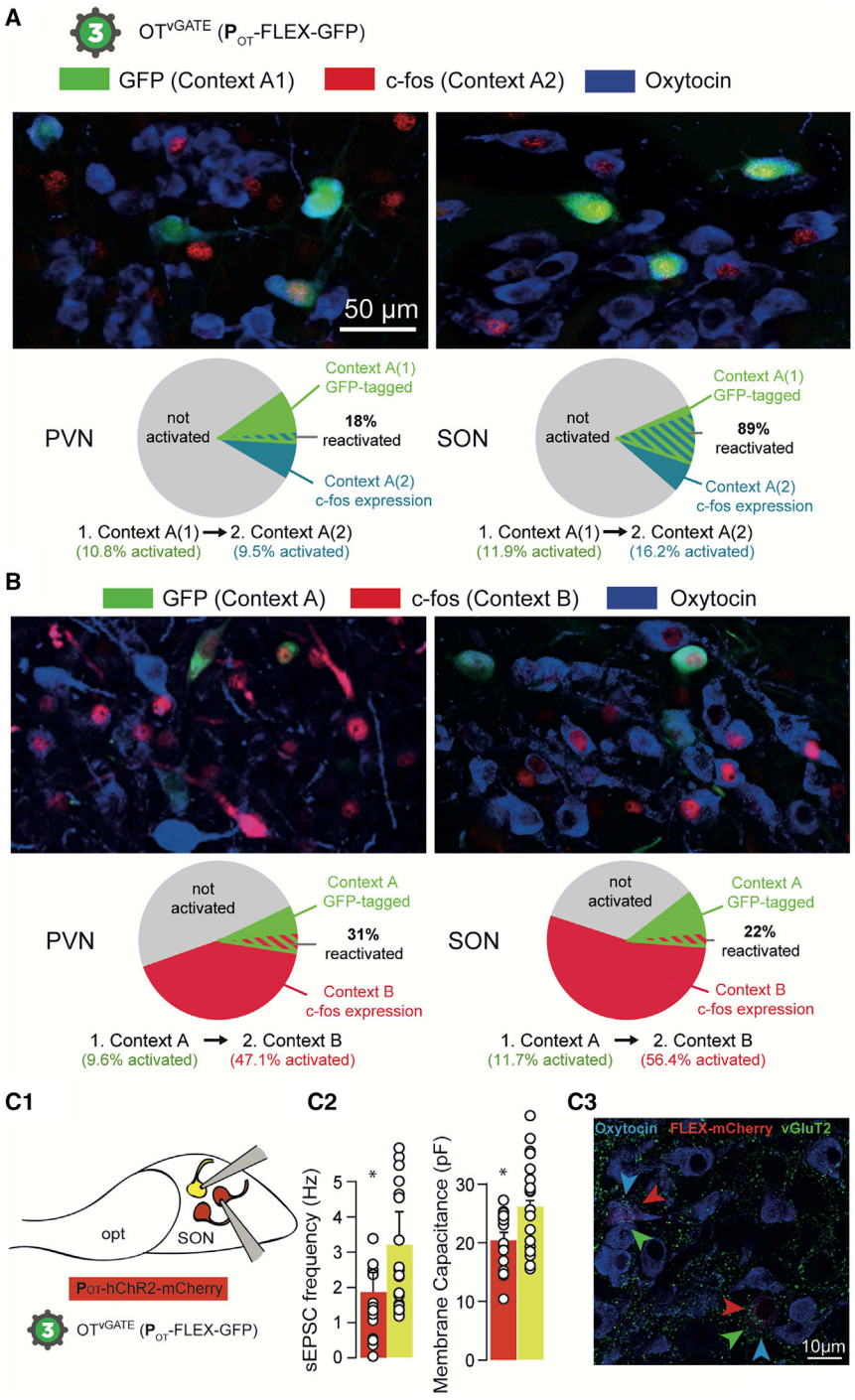

Figure 5. Context-Dependent Tagging of OT Neurons

(A and B) Percentage of OT neurons tagged in context A and reactivated after exposure to a familiar (A) or a novel (B) context. Shown are representative confocal images of the PVN and SON with an intrinsic GFP signal (green, vGATE-based tagged neurons in context A) co-stained for OT (blue) and c-*fos* (red, indicates neurons activated in context B). Pie charts show the relative numbers and percentages of GFP-positive and c-*fos*-expressing OT neurons in each hypothalamic nucleus. In the PVN, the initial exposure to context A resulted in GFP-based tagging of 10.8% of all counted OT neurons (Table S5), whereas re-exposure to the same context led to c-*fos* expression in 9.5% of OT neurons with 18% of reactivated cells (i.e., OT cells expressing GFP and c-*fos*). In the SON, exposure to context A activated 11.9% of OT neurons, and re-exposure to the same context induced c-*fos* in 16.2% of OT cells, displaying an 89% overlap in GFP and c-*fos* signals. For context B, the initial exposure activated 9.6% of OT cells in the PVN, visualized by intrinsic GFP expression, and the second exposure recruited a massive 47.1% of OT cells with a reactivated GFP-expressing fraction of 31%. In the SON, first exposure to novel context B activated 11.7% of OT neurons, whereas re-exposure to the same context resulted in drastically increased activation of 56.4% of cells but reflecting only a 22% overlap of GFP and c-*fos*.

(C) Electrophysiological properties of OT^{vGATE} versus $OT^{Constitutive}$ neurons. (C1) Experimental scheme showing OT^{vGATE} in yellow (co-localization of green and red signals) and $OT^{Constitutive}$ in red in the SON. (C2) Bar plots and individual data (dots) of spontaneous excitatory postsynaptic current (sEPSC) frequency (left) and membrane capacitance (right) recorded in OT^{vGATE} (yellow, n = 24) and $OT^{Constitutive}$ (red, n = 16). *p < 0.05, t test. (C3) VGluT2-immunoreactive puncta (green) in close vicinity of OT neurons (blue) labeled by vGATE viruses (FLEX-mCherry, red) and non-labeled OT cells of the SON. The number of vGLuT2-positive puncta in the vicinity of OT vGATE neurons is significantly higher compared with non-labeled OT neurons (p < 0.001).

hypothalamic OT cell types are reactivated during the two fear episodes. To distinguish between magnOT and parvOT neurons, we used the retrograde marker Fluorogold (FG), which labels magnOT but not parvOT cells (Naumann et al., 2000). Injecting the cocktail of vGATE viruses (virus 3, rAAV-$\mathbf{P}_{OT}$-FLEX-GFP), we found that virtually all FG-negative parvOT neurons of the PVN (parvOT neurons are not present in the SON) were labeled with GFP in context A and contained c-*fos* in context B, whereas only a small fraction (14%–20%) of FG-positive magnOT neurons of the PVN and SON labeled with GFP in context A were c-*fos* positive in context B (Figure 6A; Table S6).

Following previous findings that PVN parvOT neurons provide synaptic inputs onto OT neurons in the SON to activate magnOT neurons (Eliava et al., 2016), we aimed to silence parvOT neurons to elucidate their functional relevance in the novel context B during repeated fear exposure. To achieve this, we expressed hM4D(Gi) in a Cre-dependent manner in the PVN via a CAV2-Cre virus injected into the SON (Figure 6B) to silence parvOT inputs onto magnOT neurons. We found that silencing of parvOT

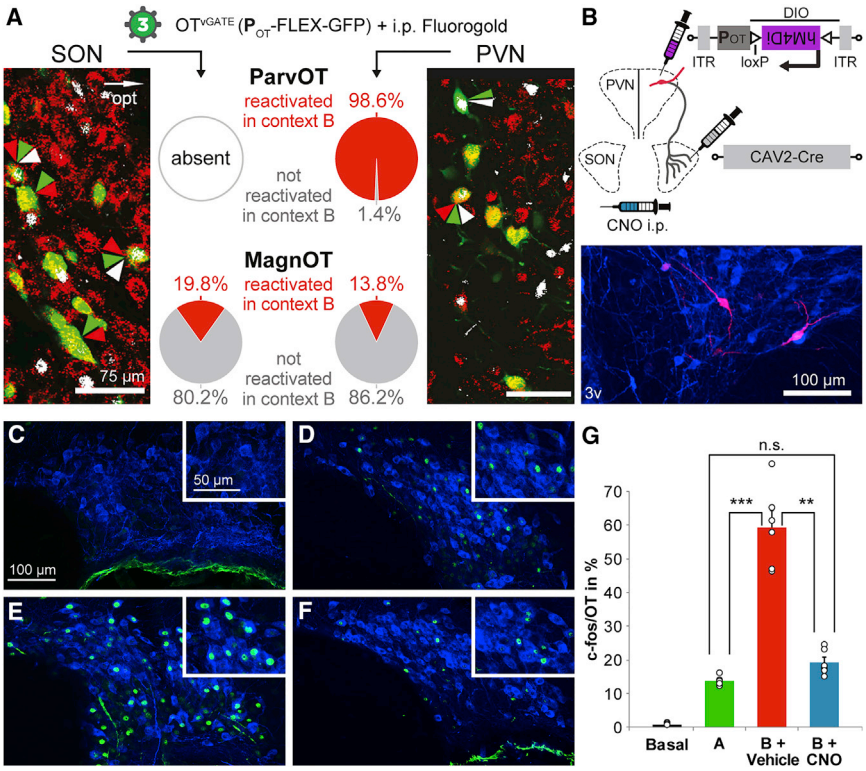

Figure 6. Pharmacogenetic Silencing of Parvocellular OT Neurons

(A) Percentage of parvOT and magnOT, tagged in context A by GFP and reactivated after exposure to context B, and representative confocal images of FG-positive (magnOT neurons, red) and FG-negative (parvOT neurons) containing intrinsic GFP and c-*fos* (white). Green arrows indicate OT neurons activated in context A (GFP), red arrows indicate magnocellular OT neurons, and white arrows indicate OT cells containing c-*fos*. Pie charts between confocal images display the distribution of c-*fos* labeling in parvOT and magnOT neurons.

(B) Experimental setup for exclusive silencing of ParvOT neurons. Animals received an injection of CAV2-Cre into the SON and Cre-dependent rAAV expressing hM4Di-mCherry under the control of the OT promoter into the PVN to specifically label parvocellular OT neurons in the PVN. The confocal image shows parvocellular OT cells (blue) expressing hM4Di-mCherry (red).

(C–F) Images of the SON of naive animals (C), rats conditioned in context A (D), and rats conditioned in context A followed by context B and treated with vehicle (E) or CNO (F).

(G) CNO treatment drastically reduced the number of c-*fos*-expressing OT neurons in the SON of rats exposed to context B. Black, control; green, exposure to context A; red, exposure to context B plus saline injection; blue, exposure to context B plus CNO injection. ***p < 0.0001, one-way ANOVA.

neurons in context B prevented the massive induction of c-*fos* expression in the SON (Figures 6C–6G; Table S6), indicating a critical role of parvOT neurons during repeated fear exposure. Similar results were obtained in the PVN (Figures S6A–S6E), suggesting that parvOT neurons might also directly or indirectly control magnOT activity within PVN neurons. To exclude that the prevented rise in c-*fos* expression was a result of CNO treatment, we subjected animals to the same paradigm, where they received CNO but were not injected with Cre-dependent hM4D(Gi) rAAV, and found no differences in c-*fos* expression in OT neurons of the SON and PVN (Figure S6F).

DISCUSSION

Here we provide first evidence that vGATE-assisted OT-tagged neurons during fear expression are sufficient for controlling fear behavior and necessary for fear extinction. Furthermore, fear experience drives enormous plasticity, mediating a shift from OT to glutamate signaling in the CeL. We propose that repeated fear exposure activates OT-ergic fear engram cells for rapid adaptive behavioral responses.

The Context-Dependent Fear Memory Engram and Its Plasticity in the Hypothalamic OT System

The hypothesis that learning-activated cell ensembles form memory engrams has received substantial attention (Kitamura et al., 2017; Liu et al., 2012; Reijmers et al., 2007). Although memory engrams have been discovered in higher brain regions such as the cortex, hippocampus, or basolateral amygdala (Kitamura et al., 2017; Liu et al., 2012), no study, to our knowledge, has addressed the potential role of the lower brain regions, such as the hypothalamus, in the modulation of fear memory. In a number of studies, the OT system has been highlighted as a key structure modulating various aspects of fear, such as acquisition, expression, and extinction.

To investigate whether OT neurons encode for context-specificity, we applied the vGATE method to identify and manipulate potential OT engram cells and labeled a small fraction (~11%–14%) of hypothalamic OT neurons by contextual FC. Remarkably, the majority of OT^{vGATE} neurons project to the CeA, and optogenetic activation of the OT neuronal axonal fibers in the CeA elicited rapid onset of unfreezing. We further found that, upon fear exposure, OT neurons show enhanced glutamatergic over OT-ergic transmission in the CeM (Figure 3D1) with increased membrane capacitance (Figure 5C2) and elevated vGluT2-levels in OT axons terminating in the CeA (Figure 5C3), consistent with previous studies (Ciocchi et al., 2010; Li et al., 2013; Penzo et al., 2015). Thus, our results provide the first evidence for fear-induced long-term plasticity (15 days) of the OT-CeL circuit. It seems indeed possible that a single episode of fear conditioning permanently alters the OT and glutamate balance, perhaps to strengthen synaptic connections for rapid response and memory maintenance. These findings support the general notion that coordinated release of slow-acting neuromodulator peptides and fast-acting amino acid transmitters could be a likely mechanism to modulate cognitive, emotional, and metabolic processes (van den Pol, 2012).

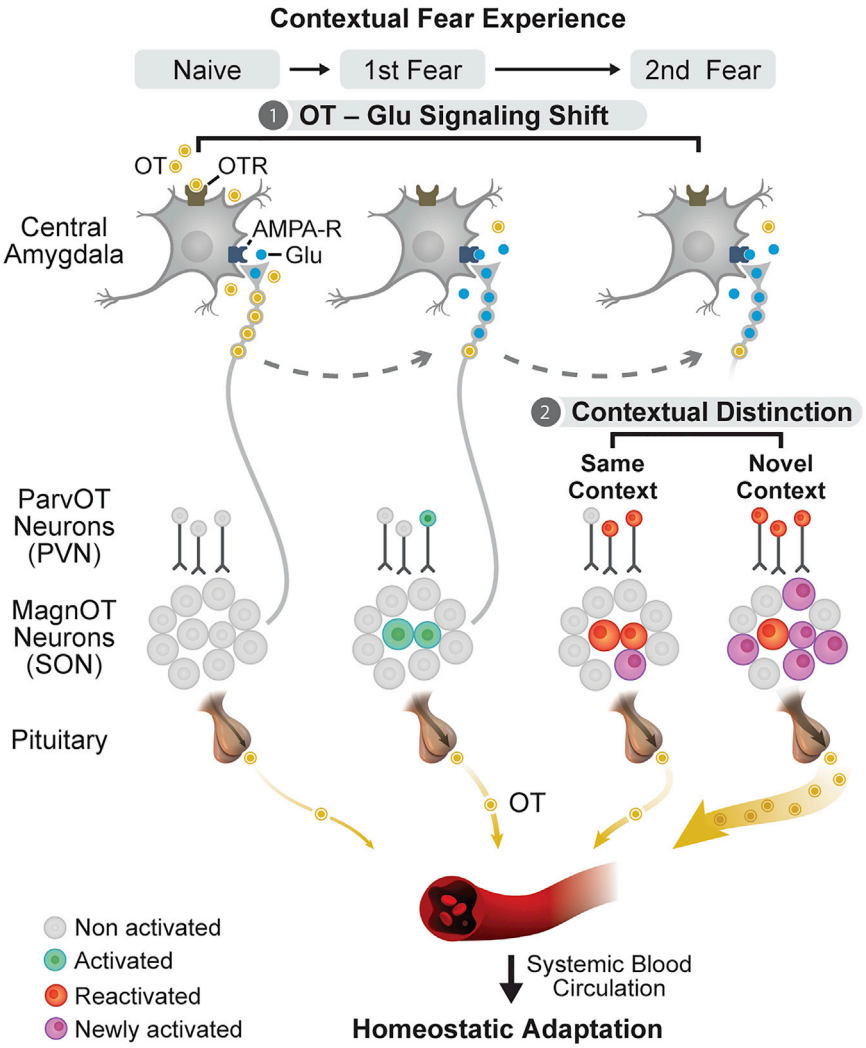

Figure 7. Context-Dependent Changes in OT Neuron Activity Following Contextual Fear Experience

The scheme represents a working hypothesis of plasticity and contextual specificity of the central OT system. At the level of OT terminals in the amygdala (top panel), the fear learning process induces drastic changes in the transmitter and neuromodulator balance: although in naive rats, OT axons predominantly release OT, in fear-experienced rats, the same axons release glutamate instead of OT. At the level of the hypothalamus (center panel), the majority of magnOT neurons in the SON exhibit context specificity and are not reactivated in a novel context. In contrast, parvOT neurons of the PVN, synapsing on SON magnOT neurons, are reactivated in a novel context and drive massive recruitment of new magnOT neurons. The massive activation of new SON OT neurons correlated with OT release to the blood, serving homeostatic adaptation to excessive stress caused by exposure to a novel fearful environment (bottom).

plays a vital role in controlling simple "contextual memory" representations for context-specific behavioral expression and the extinction phenotype.

Context-Independent Control by Parvocellular OT Neurons of the Hypothalamic OT System

OT neurons are divided into two types: magnOT and parvOT neurons. Despite their relatively low numbers (~70 neurons per rat), parvOT neurons modulate important physiological processes, such as cardiovascular functions, hunger, and pain (Althammer and Grinevich, 2017). The present study highlights the functional relevance of parvOT neurons in contextual FC because virtually all parvOT neurons that were activated in context A were also reactivated in context B, and silencing of parvOT neurons almost entirely blocked the recruitment of novel magnOT neurons in an unfamiliar context. Therefore, we hypothesize that parvOT neurons operate as a class of "master cells," orchestrating magnOT neuron activity and subsequent OT release into the blood. Although the precise role of OT neurons during fear conditioning remains to be determined, it is plausible that the coordinated activity of parvOT neurons may facilitate global priming effects and/or induce plasticity of magnOT neurons in various physiological demands (Theodosis et al., 1986; Tobin et al., 2012). In line with this, global activation of the OT system, driven by parvOT neurons, can be crucial for metabolic, autonomic, and behavioral adaption to exacerbated fear-induced stress. In our current study, the 5-fold increase in c-*fos* expression quite accurately matches the 5-fold elevation of OT levels in the blood (Figure S6A). This indicates that newly activated OT neurons in context B are magnOT cells that release the neuropeptide from the neurohypophysis into the blood.

Based on our findings, we hypothesized that OT^{vGATE} engram neurons might also be involved in fear extinction. Given the key role of CeA in fear extinction, we next investigated whether context-specific OT neuronal circuits would control context-specific fear extinction. Although inhibition of virtually all OT neurons resulted in context-independent impairment of fear extinction, inhibition of OT^{vGATE} neurons exclusively affected fear extinction in the context in which the cells had originally been labeled. These OT^{vGATE} neurons might be required for suppression of memory expression, safety cues, and priming for extinction. This could explain the unaffected fear extinction of animals in context B after silencing of OT^{vGATE} neurons that were tagged in context A, where inhibition of these fibers might no longer be relevant, because newly recruited OT neurons in a different context could compensate for the reduced release of OT in the CeA by release of this neuropeptide in other brain regions (Figures 4B2 and 4C3). Therefore, we concluded that silencing of OT^{vGATE} engram cells impaired fear extinction, demonstrating necessity, a likely result of blocking OT and glutamate-mediated neural modulation in the CeA. We propose that OT^{vGATE} cells represent a "neuromodulatory" engram that

Thus, the newly recruited OT neurons in both hypothalamic nuclei provide a massive release of OT into the peripheral circulation to regulate various physiological demands to cope with an exacerbated stress response (Yang et al., 2013).

Conclusion

We identified and validated a neuromodulatory engram composed specifically of OT cells that fulfills the key criteria of the synaptic plasticity memory hypothesis (Martin et al., 2000): sufficiency, necessity, and plasticity. We demonstrated that OT neurons of the SON participate in a fear memory engram (Figure 7), whereas parvOT neurons coordinate OT release in a context-independent manner. Our findings will facilitate the investigation of pathophysiological mechanisms underlying emotion-associated mental disorders, especially PTSD symptoms, their potential treatment by exogenous OT (Althammer et al., 2018; Frijling et al., 2014), and virus-delivered genetically based targeted therapeutic agents.

STAR★METHODS

Detailed methods are provided in the online version of this paper and include the following:

- KEY RESOURCES TABLE
- CONTACT FOR REAGENT AND RESOURCE SHARING
- EXPERIMENTAL MODEL AND SUBJECT DETAILS
  - Animals
- METHOD DETAILS
  - The vGATE system
  - Infecting rat hypothalamic neurons *in vivo* with rAAVs
  - Neuroanatomy
  - BEHAVIOR
  - Ex Vivo Electrophysiology
  - Histology
  - Measurement of Plasma ot Concentrations
- QUANTIFICATION AND STATISTICAL ANALYSIS

SUPPLEMENTAL INFORMATION

Supplemental Information can be found online at https://doi.org/10.1016/j.neuron.2019.04.029.

ACKNOWLEDGMENTS

The authors dedicate this manuscript to the memory of Professor Peter H. Seeburg (1944–2016), who generously provided us with enormous support for this 12-year-long project. This work was supported by the Max Planck Society (to M.T.H., R.S., and V.G.); the Fritz Thyssen Stiftung (to M.T.H. and V.G.); the Ministry of Economy and Business (MINECO) under the framework of the ERA-NET Neuron Cofund (to M.T.H.); Ministerio Economia, Industria y Competitividad (Spain) and FEDER (grant RTI2018-101624-B-I00 to M.T.H.); the Chica and Heinz Schaller Research Foundation (to V.G.); German Research Foundation (DFG) grant GR 3619/4-1 (to V.G.); Human Frontier Science Program RGP0019/2015 (to V.G.); the DFG within the Collaborative Research Center (SFB) 1134 (to V.G., R.S., and H.B.) and 1158 (to V.G., S.C.H., R.S., and H.B.); SNSF-DFG grant GR 3619/8-1 (to V.G.); PHC PROCOP program 32975SA (DAAD and Campus France), PICS program 07882 (CNRS), and ANR-DFG grant GR 3619/701 (to V.G. and A.C.); and FP7 career integration grant 334455, University of Strasbourg Institute for Advanced Study (USIAS) fellowship 2014-17, Foundation Fyssen research grant 2015 (to A.C.) and postdoctoral fellowship 2017-2019 (A.L.), and NARSAD young investigator grant 24821 (to A.C.). The authors thank Sadia Oumohand and Jonas Metz for help with behavioral experiments and histology; Judith Müller for cloning Cre-depended rAAVs; Barbara Kurpiers and the Interdisciplinary Neurobehavioral Core Facility of Heidelberg University for behavioral experiments performed there; Diego Benusiglio for help with statistical analysis; Inga Neumann (Regensburg), Ron Stoop (Lausanne), and Mary Lee (Bethesda) for valuable comments on the manuscript; Thomas Splettstoesser (SciStyle) for help with the preparation of figures; and Anne Seller for proofreading the manuscript.

AUTHOR CONTRIBUTIONS

Design and development of the vGATE system, M.T.H.; characterization of vGATE, M.T.H., J.-M.W., G.K.D., and I.B.; project conception, M.T.H., A.C., and V.G.; implementation of other methodologies, M.T.H., J.-M.W., R.H., M.E.L., R.S., and H.B.; *ex vivo* patch-clamp electrophysiology, S.G., J.W., P.D., Y.T., X.L., and A.C.; viral injections, F.A., M.S.d.G., and S.G.; fear behavior, F.A., M.S.d.G., S.G., D.K., A.J., A.R., J.S., and C.P.; immunohistochemistry, F.A., M.S.d.G., A.L., M.E., and H.S.K.-B.; HPLC MS/MS, V.C. and Y.G.; data analysis, F.A., M.S.d.G., S.G., A.R., J.-M.W., and A.C.; confocal microscopy, F.A., M.E.L., M.S.d.G., and A.L.; manuscript preparation, M.T.H., A.C., and V.G.; extended manuscript preparation, F.A., H.S.K.-B., R.H., S.C.H., R.S., H.B., A.C., M.T.H., and V.G.; supervision, M.T.H., A.C., and V.G.; project administration, M.T.H., A.C., and V.G.; funding acquisition, M.T.H., A.C., and V.G.

DECLARATION OF INTERESTS

The authors declare no competing interests.

Received: May 18, 2018
Revised: October 8, 2018
Accepted: April 18, 2019
Published: May 16, 2019

REFERENCES

Althammer, F., and Grinevich, V. (2017). Diversity of oxytocin neurons: beyond magno- and parvocellular cell types? J. Neuroendocrinol. Published online October 12, 2017. https://doi.org/10.1111/jne.12549.

Althammer, F., Jirikowski, G., and Grinevich, V. (2018). The oxytocin system of mice and men-Similarities and discrepancies of oxytocinergic modulation in rodents and primates. Peptides *109*, 1–8.

Bru, T., Salinas, S., and Kremer, E.J. (2010). An update on canine adenovirus type 2 and its vectors. Viruses *2*, 2134–2153.

Cetin, A., Komai, S., Eliava, M., Seeburg, P.H., and Osten, P. (2006). Stereotaxic gene delivery in the rodent brain. Nat. Protoc. *1*, 3166–3173.

Ciocchi, S., Herry, C., Grenier, F., Wolff, S.B., Letzkus, J.J., Vlachos, I., Ehrlich, I., Sprengel, R., Deisseroth, K., Stadler, M.B., et al. (2010). Encoding of conditioned fear in central amygdala inhibitory circuits. Nature *468*, 277–282.

Dogbevia, G.K., Marticorena-Alvarez, R., Bausen, M., Sprengel, R., and Hasan, M.T. (2015). Inducible and combinatorial gene manipulation in mouse brain. Front. Cell. Neurosci. *9*, 142.

Dogbevia, G.K., Roβmanith, M., Sprengel, R., and Hasan, M.T. (2016). Flexible, AAV-equipped Genetic Modules for Inducible Control of Gene Expression in Mammalian Brain. Mol. Ther. Nucleic Acids *5*, e309.

Ehrlich, I., Humeau, Y., Grenier, F., Ciocchi, S., Herry, C., and Lüthi, A. (2009). Amygdala inhibitory circuits and the control of fear memory. Neuron *62*, 757–771.

Eliava, M., Melchior, M., Knobloch-Bollmann, H.S., Wahis, J., da Silva Gouveia, M., Tang, Y., Ciobanu, A.C., Triana Del Rio, R., Roth, L.C., Althammer, F., et al. (2016). A New Population of Parvocellular Oxytocin Neurons Controlling Magnocellular Neuron Activity and Inflammatory Pain Processing. Neuron *89*, 1291–1304.

Fadok, J.P., Krabbe, S., Markovic, M., Courtin, J., Xu, C., Massi, L., Botta, P., Bylund, K., Müller, C., Kovacevic, A., et al. (2017). A competitive inhibitory circuit for selection of active and passive fear responses. Nature *542*, 96–100.

Frijling, J.L., van Zuiden, M., Koch, S.B., Nawijn, L., Goslings, J.C., Luitse, J.S., Biesheuvel, T.H., Honig, A., Bakker, F.C., Denys, D., et al. (2014). Efficacy of oxytocin administration early after psychotrauma in preventing the development of PTSD: study protocol of a randomized controlled trial. BMC Psychiatry *14*, 92.

Gomez, J.L., Bonaventura, J., Lesniak, W., Mathews, W.B., Sysa-Shah, P., Rodriguez, L.A., Ellis, R.J., Richie, C.T., Harvey, B.K., Dannals, R.F., et al. (2017). Chemogenetics revealed: DREADD occupancy and activation via converted clozapine. Science *357*, 503–507.

Grund, T., Goyon, S., Li, Y., Eliava, M., Liu, H., Charlet, A., Grinevich, V., and Neumann, I.D. (2017). Neuropeptide S Activates Paraventricular Oxytocin Neurons to Induce Anxiolysis. J. Neurosci. *37*, 12214–12225.

Guenthner, C.J., Miyamichi, K., Yang, H.H., Heller, H.C., and Luo, L. (2013). Permanent genetic access to transiently active neurons via TRAP: targeted recombination in active populations. Neuron *78*, 773–784.

Hamamura, M., Leng, G., Emson, P.C., and Kiyama, H. (1991). Electrical activation and c-fos mRNA expression in rat neurosecretory neurones after systemic administration of cholecystokinin. J. Physiol. *444*, 51–63.

Heidbreder, C.A., and Groenewegen, H.J. (2003). The medial prefrontal cortex in the rat: evidence for a dorso-ventral distinction based upon functional and anatomical characteristics. Neurosci. Biobehav. Rev. *27*, 555–579.

Herry, C., Ferraguti, F., Singewald, N., Letzkus, J.J., Ehrlich, I., and Lüthi, A. (2010). Neuronal circuits of fear extinction. Eur. J. Neurosci. *31*, 599–612.

Katoh, A., Fujihara, H., Ohbuchi, T., Onaka, T., Young, W.S., 3rd, Dayanithi, G., Yamasaki, Y., Kawata, M., Suzuki, H., Otsubo, H., et al. (2010). Specific expression of an oxytocin-enhanced cyan fluorescent protein fusion transgene in the rat hypothalamus and posterior pituitary. J. Endocrinol. *204*, 275–285.

Kessler, R.C., and Bromet, E.J. (2013). The epidemiology of depression across cultures. Annu. Rev. Public Health *34*, 119–138.

Kitamura, T., Ogawa, S.K., Roy, D.S., Okuyama, T., Morrissey, M.D., Smith, L.M., Redondo, R.L., and Tonegawa, S. (2017). Engrams and circuits crucial for systems consolidation of a memory. Science *356*, 73–78.

Knobloch, H.S., Charlet, A., Hoffmann, L.C., Eliava, M., Khrulev, S., Cetin, A.H., Osten, P., Schwarz, M.K., Seeburg, P.H., Stoop, R., and Grinevich, V. (2012). Evoked axonal oxytocin release in the central amygdala attenuates fear response. Neuron *73*, 553–566.

Koohi, M.K., Ivell, R., and Walther, N. (2005). Transcriptional activation of the oxytocin promoter by oestrogens uses a novel non-classical mechanism of oestrogen receptor action. J. Neuroendocrinol. *17*, 197–207.

LeDoux, J. (2007). The amygdala. Curr. Biol. *17*, R868–R874.

Letzkus, J.J., Wolff, S.B., Meyer, E.M., Tovote, P., Courtin, J., Herry, C., and Lüthi, A. (2011). A disinhibitory microcircuit for associative fear learning in the auditory cortex. Nature *480*, 331–335.

Li, H., Penzo, M.A., Taniguchi, H., Kopec, C.D., Huang, Z.J., and Li, B. (2013). Experience-dependent modification of a central amygdala fear circuit. Nat. Neurosci. *16*, 332–339.

Liu, X., Ramirez, S., Pang, P.T., Puryear, C.B., Govindarajan, A., Deisseroth, K., and Tonegawa, S. (2012). Optogenetic stimulation of a hippocampal engram activates fear memory recall. Nature *484*, 381–385.

Lütcke, H., Murayama, M., Hahn, T., Margolis, D.J., Astori, S., Zum Alten Borgloh, S.M., Göbel, W., Yang, Y., Tang, W., Kügler, S., et al. (2010). Optical recording of neuronal activity with a genetically-encoded calcium indicator in anesthetized and freely moving mice. Front. Neural Circuits *4*, 9.

Martin, S.J., Grimwood, P.D., and Morris, R.G. (2000). Synaptic plasticity and memory: an evaluation of the hypothesis. Annu. Rev. Neurosci. *23*, 649–711.

Mobbs, D., Hagan, C.C., Dalgleish, T., Silston, B., and Prévost, C. (2015). The ecology of human fear: survival optimization and the nervous system. Front. Neurosci. *9*, 55.

Naumann, T., Härtig, W., and Frotscher, M. (2000). Retrograde tracing with Fluoro-Gold: different methods of tracer detection at the ultrastructural level and neurodegenerative changes of back-filled neurons in long-term studies. J. Neurosci. Methods *103*, 11–21.

Penzo, M.A., Robert, V., Tucciarone, J., De Bundel, D., Wang, M., Van Aelst, L., Darvas, M., Parada, L.F., Palmiter, R.D., He, M., et al. (2015). The paraventricular thalamus controls a central amygdala fear circuit. Nature *519*, 455–459.

Reijmers, L.G., Perkins, B.L., Matsuo, N., and Mayford, M. (2007). Localization of a stable neural correlate of associative memory. Science *317*, 1230–1233.

Rhodes, C.H., Morrell, J.I., and Pfaff, D.W. (1981). Immunohistochemical analysis of magnocellular elements in rat hypothalamus: distribution and numbers of cells containing neurophysin, oxytocin, and vasopressin. J. Comp. Neurol. *198*, 45–64.

Ryan, T.J., Roy, D.S., Pignatelli, M., Arons, A., and Tonegawa, S. (2015). Memory. Engram cells retain memory under retrograde amnesia. Science *348*, 1007–1013.

Schilling, K., Luk, D., Morgan, J.I., and Curran, T. (1991). Regulation of a fos-lacZ fusion gene: a paradigm for quantitative analysis of stimulus-transcription coupling. Proc. Natl. Acad. Sci. USA *88*, 5665–5669.

Somponpun, S.J., and Sladek, C.D. (2003). Osmotic regulation of estrogen receptor-beta in rat vasopressin and oxytocin neurons. J. Neurosci. *23*, 4261–4269.

Stachniak, T.J., Ghosh, A., and Sternson, S.M. (2014). Chemogenetic synaptic silencing of neural circuits localizes a hypothalamus→midbrain pathway for feeding behavior. Neuron *82*, 797–808.

Swanson, L.W., and Kuypers, H.G. (1980). The paraventricular nucleus of the hypothalamus: cytoarchitectonic subdivisions and organization of projections to the pituitary, dorsal vagal complex, and spinal cord as demonstrated by retrograde fluorescence double-labeling methods. J. Comp. Neurol. *194*, 555–570.

Swanson, L.W., and Sawchenko, P.E. (1983). Hypothalamic integration: organization of the paraventricular and supraoptic nuclei. Annu. Rev. Neurosci. *6*, 269–324.

Theodosis, D.T., Montagnese, C., Rodriguez, F., Vincent, J.D., and Poulain, D.A. (1986). Oxytocin induces morphological plasticity in the adult hypothalamo-neurohypophysial system. Nature *322*, 738–740.

Tobin, V., Leng, G., and Ludwig, M. (2012). The involvement of actin, calcium channels and exocytosis proteins in somato-dendritic oxytocin and vasopressin release. Front. Physiol. *3*, 261.

Tovote, P., Fadok, J.P., and Lüthi, A. (2015). Neuronal circuits for fear and anxiety. Nat. Rev. Neurosci. *16*, 317–331.

van den Pol, A.N. (2012). Neuropeptide transmission in brain circuits. Neuron *76*, 98–115.

Viviani, D., Charlet, A., van den Burg, E., Robinet, C., Hurni, N., Abatis, M., Magara, F., and Stoop, R. (2011). Oxytocin selectively gates fear responses through distinct outputs from the central amygdala. Science *333*, 104–107.

Yang, H.P., Wang, L., Han, L., and Wang, S.C. (2013). Nonsocial functions of hypothalamic oxytocin. ISRN Neurosci. *2013*, 179272.

Please cite this article in press as: Hasan et al., A Fear Memory Engram and Its Plasticity in the Hypothalamic Oxytocin System, Neuron (2019), https://doi.org/10.1016/j.neuron.2019.04.029

STAR★METHODS

KEY RESOURCES TABLE

REAGENT OR RESOURCE	SOURCE	IDENTIFIER
Antibodies		
Chicken anti-GFP primary antibody	Abcam	ab13970
Mouse NeuN primary antibody	Chemicon	A60
Rabbit vGluT2 primary antibody	Synaptic systems	135 103
Rabbit anti-dsRed primary antibody	Clontech	632496
Rabbit anti-Fluorogold primary antibody	Milipore	AB153
Guinea-pig anti-Fluorogold primary antibody	Protos Biotech Corp	NM-101
Rabbit c-fos polyclonal primary antibody	Santa-Cruz	sc-7202
Mouse monoclonal anti-OT primary antibody	Provided by Dr. Harold Gainer	PS 38
Rabbit polyclonal anti-CRH primary antibody	Peninsula Labs	T-4035.0500
Rat monoclonal anti-Somatostatin primary antibody	Chemicon	MAB345
Rabbit polyclonal anti-vGluT2 primary antibody	SYSY	135403
Bacterial and Virus strains		
$(tetO)_7$-**P**$_{c\text{-}fos}$-rtTA AAV 1/2	This paper	N/A
YC3.60-**P**$_{tet}$bi-Cre AAV 1/2	This paper	N/A
P$_{OT}$-FLEX-hChr2-mCherry AAV 1/2	Eliava et al., 2016	N/A
CAV2-Cre	Bru et al., 2010	N/A
P$_{OT}$-Venus AAV 1/2	Knobloch et al., 2012	N/A
P$_{OT}$-FLEX-GFP AAV 1/2	Eliava et al., 2016	N/A
P$_{OT}$-FLEX-hM4D(Gi)-mCherry AAV 1/2	Eliava et al., 2016	N/A
Chemicals, Peptides, and Recombinant Proteins		
Fluorogold	Santa-Cruz	sc-358883
Oxytocin Receptor Antagonist	Santa-Cruz	L-368,899
Doxycycline	Cayman Chemical Company	14422
Clozapine-N-Oxide	Tocris Bioscience	4936
NBQX	Abcam	Ab120018
dOVT	Bachem	H2908
Retrobeads	Lumaflour	N/A
Experimental Models: Organisms/Strains		
Rattus Norvegicus (Wistar)	Janvier	N/A
Recombinant DNA		
$(tetO)_7$-**P**$_{c\text{-}fos}$-rtTA	This paper	N/A
YC3.60-**P**$_{tet}$bi-Cre	This paper	N/A
P$_{OT}$-FLEX-hChr2-mCherry	Eliava et al., 2016	N/A
P$_{OT}$-Venus	Knobloch et al., 2012	N/A
P$_{OT}$-FLEX-GFP	Eliava et al., 2016	N/A
P$_{OT}$-FLEX-hM4D(Gi)-mCherry	Eliava et al., 2016	N/A
Software and Algorithms		
Graphpad prism 7.0	https://www.graphpad.com/	N/A
Fiji	http://www.imagej.net/Fiji	N/A
Adobe Photoshop CS5	https://www.adobe.com/	N/A
Adobe Illustrator 16.05	https://www.adobe.com/	N/A
Panlab Fear conditioning software	https://www.panlab.com/	N/A

(*Continued on next page*)

Continued

REAGENT OR RESOURCE	SOURCE	IDENTIFIER
Other		
Optic fiber implants	https://www.thorlabs.com/	CFMLC52L02
Laser cables for optogenetics	https://www.thorlabs.com/	M106L01
Guide cannula 5.8mm	http://www.bilaney.com/plastics-one/	C313G/spc
Cannula dummy cap	http://www.bilaney.com/plastics-one/	C313DC/1/spc
Internal cannula	http://www.bilaney.com/plastics-one/	C313I/spc
473nm Blue Laser Generator	http://www.dreamlasers.com	SDL-473-XXXT
Programmable Pulse Stimulator (A.M.P.I.)	http://www.ampi.co.il	Master-9

CONTACT FOR REAGENT AND RESOURCE SHARING

Requests for vGATE tools should be directed to mazahir.t.hasan@gmail.com. For other tools and reagents, contact v.grinevich@dkfz-heidelberg.de.

EXPERIMENTAL MODEL AND SUBJECT DETAILS

Animals

Anatomical, electrophysiological, optogenetic and behavioral studies were performed with female Wistar rats purchased from Janvier, France (8-10 weeks old on arrival at our facility). All rats were housed under standard conditions with *ad libitum* access to food and water. All experiments have been approved by the German Animal Ethics Committee of the Baden Württemberg (licenses numbers 35-9185.81/G-24/12, 35-9185.81/G-26/15 and 35-9185.81G-102/17) and the French Ministry of Research (APAFIS#3668-2016011815445431 v2).

METHOD DETAILS

The vGATE system

Generation and cloning

We engineered a synthetic c-*fos* promoter linked to its first exon (Exon 1; (Schilling et al., 1991) with ATGs in the Exon 1 converted to TTGs by site directed mutagenesis and heptamerized tetracycline (tet) operators, $(tetO)_7$, added upstream of it. These operators drive the expression of a humanized reverse tet transactivator (rtTA) (Dogbevia et al., 2015) named $(tetO)_7$-$\mathbf{P}_{fos}$-rtTA. The entire cassette was subsequently cloned in a plasmid to produce recombinant adeno-associated viruses (rAAVs) packaged with serotype 1 and 2 (Dogbevia et al., 2015) to generate Virus1 (rAAV-$(tetO)_7$-$\mathbf{P}_{fos}$-rtTA). Next, an AAV equipped with bidirectional tet promoter (P_{tet}bi) expressing the Cre-recombinase was linked to a genetically-encoded calcium indicator (YC3.60) (Virus 2, rAAV-$\mathbf{P}_{tet}$bi-Cre/YC3.60, (Lütcke et al., 2010)). As the last component of our viral technique (Virus 3), we generated rAAVs under the OT promoter to drive expression of hChR2-mCherry, GFP or hM4D(Gi)-mCherry (Eliava et al., 2016; Grund et al., 2017) in a Cre-dependent manner. The entire system comprising rAAV-$(tetO)_7$-$\mathbf{P}_{fos}$-rtTA (Virus 1), as the key element of the system, combined with rAAV-$\mathbf{P}_{tet}$bi-Cre/YC3.60 (Virus 2) and the Cre-dependent 'FLEX' viruses (Virus 3, see Key Resources Table) for '**v**irus-delivered, **G**enetic **A**ctivity-dependent **T**agging of cell **E**nsembles' or vGATE. In the vGATE method, the c-*fos* promoter drives rtTA expression only when neurons are activated. The rtTA generated by transient c-*fos* promoter activity binds to the upstream $(tetO)_7$ only in the presence of Dox. This way, the rtTA drives its own expression, thus establishing an autoregulatory loop, even when the induced c-*fos* promoter activity declines to baseline levels as neuronal activity subsides. Therefore, only in the presence of Dox, the rtTA can activate the expression of the bidirectional tet promoter ($\mathbf{P}_{tet}$bi) to express any gene of choice, for example, the Cre recombinase, for permanent tagging of activated cells via a Cre-dependent FLEX cassette.

Validating in cultured neurons

Dissociated rat hippocampal cultured neurons were treated with two viruses (rAAV-$(tetO)_7$-$\mathbf{P}_{fos}$-rtTA + rAAV-$\mathbf{P}_{tet}$bi-Cre/tdTOM) for two weeks. Afterward, cells were treated with bicuculline (bic) for 20 min and replaced with fresh medium supplemented with Dox (1 μg/ml) for 24 h. Only in the presence of bic and Dox, a strong rtTA signal was detected by immunohistochemistry (Figure S1, bottom panel). By live fluorescence imaging of fixed cells, rtTA-dependent tdTOM expression was also clearly detected in +bic/+Dox treated cells. In a few neurons, however, tdTOM expression was also detected under condition of –bic/+Dox. This is likely a result of spontaneous activity in some neurons. Western blot analyses validated tdTOM expression (Figure S1).

Novelty of the method

We describe here a genetic method (vGATE) that uses c-*fos* promoter elements to drive expression of a reverse tetracycline transactivator (rtTA). The key novelty of our method is that the 'recording period' can be rapidly opened within a few hours by a single

intraperitoneal Dox injection before the tagging of activated neurons. In previous methodological studies, we carefully characterized, both *ex vivo* and *in vivo*, the regulation of Dox-controlled gene expression by rtTA expressed under a human synapsin promoter (Dogbevia et al., 2015; Dogbevia et al., 2016). We determined an optimal Dox concentration for *in vivo* application, and the time course of gene activation and inactivation by a single intraperitoneal Dox injection. In our previous studies, we found that the bidirectional Tet promoter ($\mathbf{P}_{tet}$bi) has highly reduced leakiness (Dogbevia et al., 2016) compared to the uni-directional Tet promoter ($\mathbf{P}_{tet}$) (Dogbevia et al., 2015). Indeed, $\mathbf{P}_{tet}$ is very leaky (Dogbevia et al., 2015), due to its close proximity close to an inverted terminal repeat (ITR) of AAV, which appears to have intrinsic enhancer-like activity (Dogbevia et al., 2015). This raises potential concerns that AAVs equipped with a uni-directional tet promoter ($\mathbf{P}_{tet}$) might be leaky enough to non-specifically tag non-engram cells. With these considerations, we characterized the vGATE method both *ex vivo* and *in vivo*. The vGATE method is very tightly controlled and highly flexible; different combination of gene modules in rAAVs can be simultaneously delivered to the targeted brain region(s). With this approach, we performed selective and cell-type-specific tagging of OT neurons activated during contextual fear learning and expressed in the tagged neurons gene(s)-of-interest for pharmacogenetic and optogenetic manipulations, while others might easily target different neuronal populations.

Different methods exist to induce time-dependent conditional protein expression, namely the TetTag (Reijmers et al., 2007) and the TRAP (Guenthner et al., 2013) methods. The TetTag method drives tTA expression under c-*fos* and animals have to be fed Dox to keep the system inactive. However, to open the recording period, TeTag animals have to be switched to diet without Dox for a few days before performing learning-dependent neuronal labeling. However, this non-recording period of a few days is sensitive for non-specific labeling of neurons. In the case of vGATE, the presence of Dox is requested to activate detectable gene expression within a few hours and achieved the maximum expression after 24 h (Dogbevia et al., 2015, 2016) and gene expression is switched-off in 6 days (Dogbevia et al., 2016). In a previous systematic study (Dogbevia et al., 2016), we found similar time course of 6 days to ''re-activate'' (with the tTA system) by Dox removal and ''activate'' (with the rtTA system) gene expression by Dox addition. The discrepancy for 3 days for Dox clearance by others using the tTA system is likely due to the sensitivity of the detection method; we used a highly sensitive reporter, the firefly luciferase, for gene expression assay as a proxy for Dox clearance from the brain (Dogbevia et al., 2016), while other labs use GFP (Liu et al., 2012), which are much less sensitive.

In the TRAP method, the inducer, tamoxifen, is needed to facilitate release cytoplasmic ER-Cre for transport to the nucleus to permanently tag neurons by Cre/loxP dependent gene modules. However, TRAP is in itself leaking, since it is known that a fraction of ER-Cre can already move to the nucleus even without tamoxifen treatment. There is even a bigger concern that tamoxifen as a selective estrogen modulator might interfere with various estrogen-sensitive cell types in the brain. The use of tamoxifen is especially critical for OT neurons, which are sensitive for estrogens (Somponpun and Sladek, 2003) and tamoxifen itself triggers the activity of the OT gene promoter (Koohi et al., 2005). Finally, tamoxifen induces c-*fos* expression in OT neurons (F.A. and V.G., unpublished data), thereby precluding the use of the ER-Cre method for this particular neuron type. With our novel vGATE technique, we achieved highly specific labeling of OT neurons and precise temporal control, which we believe to be superior to other comparable, c-*fos* based tagging methods. Therefore, the development of the vGATE method should be able to overcomes the key inherent concerns of the previous two main strategies to induce time-dependent conditional protein expression.

Infecting rat hypothalamic neurons *in vivo* with rAAVs

Cloning of the OT promoter, as well as the production and purification of rAAVs, has been previously described (Knobloch et al., 2012). rAAV genomic titers were determined with QuickTiter AAV Quantitation Kit (Cell Biolabs, San Diego, California, USA) and RT-PCR using the ABI 7700 cycler (Applied Biosystems, California, USA). rAAVs titers were between 10^{10} - 10^{11} genomic copies per 1 μl. Infection of OT neurons was achieved by complementing the two viruses indicated above by an rAAV, driving genes of interest (Venus, hChR2-mCherry, FLEX-GFP, FLEX-hM4D and hM4D(Gi). A cocktail of the three rAAVs (i.e., rAAV-$(tetO)_7$-$\mathbf{P}_{fos}$-rtTA, rAAV-$\mathbf{P}_{tet}$bi-Cre/YC3.60, and rAAV-$\mathbf{P}_{OT}$-Venus) was injected bilaterally into the hypothalamic nuclei, the PVN and SON, using a previously described protocol (Knobloch et al., 2012).

Neuroanatomy

To trace, label and manipulate the hypothalamus-amygdala connections, rAAVs expressing vGATE viruses were injected into the PVN and SON. Alternatively, CAV2-Cre was injected into the SON, while the Cre-dependent ''FLEX'' $\mathbf{P}_{OT}$-hM4D(Gi) rAAV was injected into the PVN to specifically label and manipulate parvOT neurons. After transcardial perfusion with 4% PFA, brains were sectioned and stained with antibodies against OT, vGluT2, GFP, FG and dsRed. Images for qualitative and quantitative analyses were taken on the confocal microscope Leica SP5.

BEHAVIOR

Salt loading

To validate the vGATE system *in vivo*, we performed salt-loading (SL) as a stimulus to activate c-*fos* expression in OT neurons (Katoh et al., 2010). Here, we used a mixture of two rAAVs (rAAV-$(tetO)_7$-$\mathbf{P}_{fos}$-rtTA and rAAV-$\mathbf{P}_{OT}$-Venus) and co-injected them unilaterally into the SON of rats. The animals were divided into four groups (n = 3/group): Group 1 (Untreated control animals (-Dox/-SL)), Group 2 (-Dox/+SL, 7 days with SL (2% NaCl in drinking water), Group 3 (+Dox/-SL, normally hydrated animals, which received single Dox i.p.

injection) and Group 4 (+Dox/+SL, animals received a single i.p. injection of Dox on the 5th day of SL and were kept under SL for 2 more days before being sacrificed). Expression patterns of the individual groups are depicted in Figure 1D.

Contextual fear conditioning and optogenetics

We used a mixture of three vGATE viruses as depicted (Figure 1A). Two weeks after the viral infection, adult female rats were subjected to either a 3-day (single fear) or 15-day (double fear) contextual fear conditioning protocol, comprising a conditioning session on the first 2 days and a recall session on the 3rd day (Figure 2A). All sessions lasted for 20 min with 7 random foot shocks (1.6mA, 1 s) dispersed between the 10th and 17th min of protocol during the fear conditioning session.

As shown in Figure 2A, animals were treated with Dox (5 mg/kg b.w., i.p.) 24 h after the 2nd day of fear acquisition to tag OT neurons activated during fear expression. The experimental group (animals injected with the vGATE system: rAAV-(tetO)$_7$-**P**$_{fos}$-rtTA + rAAV-**P**$_{tet}$bi-Cre/YC3.60 + rAAV-**P**$_{OT}$-FLEX-hChR2-mCherry) received another re-conditioning session (double fear), two weeks after Dox injection and recovery, for one day, to achieve a higher level of freezing (above 50 s/min) and 24 h later were tested for the recall of fear behavior with blue light (BL) illumination of the CeA. The CeA was illuminated bilaterally with BL (473 nm, 10 ms pulse, 20 s duration, 30 Hz) via 200 μm optical fibers from Thorlabs (BFL37 200) at the 10th min of the recall session. The rats were evaluated for freezing responses and freezing durations were measured through freezing software (Panlab) and manually through an offline video in addition. In Figure 2C, the 2 different graphs display the average freezing time per minute in the corresponding groups (OT^{Constitutive} and OT^{vGATE}) before and after BL illumination. The black bars (control) show the average freezing times in minutes immediately prior to the BL illumination, whereas the gray bars (BL) indicate the average freezing times per minute during the minute in which the BL-induced onset of the unfreezing effect (i.e., where the first signs of mobility appear). All groups of animals were sacrificed 90 min after the start of the optogenetic session.

Estimation of the estrous cycle

To monitor ovarian cycle, we performed vaginal smear collections. Animals in metestus, proestrus and estrus phases were excluded from experiments and reintroduced once they reached diestrus.

Pharmacogenetics (DREADD) and fear extinction in Contexts A and B

In this experiment, animals were subjected to a series of fear conditioning and fear extinction paradigms that we performed in two different contexts (A and B). For this purpose, two visually distinct contextual fear conditioning chambers were used, which were comparable in size, shape of the grid and power of the electrical shocks (1.6 mA). The chambers were located in two different institutes (chamber A, Max Planck Institute of Medical Research (MPI), Heidelberg, Panlab; chamber B, Interdisciplinary Neurobehavioral Core (INBC), Heidelberg, Med Associates) and the animals were exposed to them for the first time in both cases. Animals were injected with **P**$_{OT}$-hM4D(Gi) (OT^{Constitutive}) or rAAV-(tetO)$_7$-**P**$_{fos}$-rtTA, rAAV-**P**$_{tet}$bi-Cre/YC3.60 + rAAV-**P**$_{OT}$-FLEX-hM4D(Gi) (OT^{vGATE}) and subjected to the experimental procedure after recovery and handling. For the contextual fear conditioning, animals were placed in a fear conditioning chamber (Panlab, Harvard Apparatus) with a metal grid for application of electrical foot shocks (1.6 mA). We used a 3-day fear conditioning protocol (2 days shock, 1 day testing, each 20 min) to fear condition the animals. On the first two days, the animals, after a 10 min habituation period, received 7 electrical foot shocks within 7 min (randomly distributed, on average 1 shock per min), followed again by 3 min without shocks. For activation of the viral system, animals received Dox (5 mg/kg b.w., i.p.) on day 3 of the fear conditioning (24 h after the 2nd shock day of the first round of fear conditioning). On the fourth day (24 h after injection), animals were placed in the same box for 20 min without any shocks. The experiment was recorded with a video camera and sensors in the grid measured the total movement of the animals during the procedure. After a 2-week break (Dox clearance and viral expression) animals were exposed to the box in a second session. Here, we used a 5-day fear extinction protocol with one re-conditioning day (in order to maintain a high level of freezing (above 50 s/min) and identical in all groups) and 4 testing days. Due to the 2-week interval in between the two rounds, animals received electrical shocks on the first day (recall session), followed by 4 days on which the animals were placed in the box for 40 min each without any shocks (extinction sessions). Animals expressing the hMD4D(Gi) receptor in all OT neurons (OT^{Constitutive}) or tagged OT neurons (OT^{vGATE}) received a daily injection of Clozapine (3 mg/kg bw i.p., Tocris Bioscience, Bristol, UK, dissolved in 1xPBS) 30 min prior to placing them into the Context A chamber. The control groups (OT^{Constitutive} and OT^{vGATE}) received the same volume of 0.9% NaCl solution. After the first round of fear extinction in Context A, animals were transferred to Context B. Here, an additional round of fear extinction was performed, which comprised two shock sessions followed by 4 consecutive daily extinction sessions, 40 min prior to which the animals received a daily injection of CNO (Figure 4A), whereas the control group received the same volume of 0.9% NaCl solution 40 min prior to the start of the session. All animals were sacrificed and perfused 90 mins after the fear conditioning session in Context B. In the two control groups, the time of freezing in both contexts was almost identical (Figure S4B). Therefore, for the sake of simplicity, only the freezing time of OT^{Constitutive} and OT^{vGATE} control groups in Context A is depicted in Figures 4B1 and 4B2.

Context A versus Context A - mapping of OT neuronal activity via GFP followed by immunostaining for c-fos

Animals were injected in all nuclei with the vGATE system (rAAV-(tetO)$_7$-**P**$_{fos}$-rtTA + rAAV-**P**$_{tet}$bi-Cre/YC3.60 + rAAV-**P**$_{OT}$-FLEX-GFP) and subjected to the 3-day contextual fear conditioning paradigm after recovery and handling. Following the first two shock sessions, animals received Dox (5 mg/kg b.w., i.p.) on the 3rd day of the fear conditioning paradigm. On the 4th day, animals were exposed to the fear conditioning chamber, this time without electrical shocks. Two weeks after the 1st round of fear conditioning in Context A (1), the animals were exposed to Context A(2) for a second time, where they underwent an additional session of fear conditioning. All animals were sacrificed 90 min after the beginning of the test session in Context A (2).

Context A versus Context B - mapping of OT neuronal activity via GFP followed by immunostaining for c-fos

Animals were injected with the vGATE system into all nuclei (rAAV-$(tetO)_7$-$\mathbf{P}_{fos}$-rtTA + rAAV-$\mathbf{P}_{tet}$bi-Cre/YC3.60 + rAAV-$\mathbf{P}_{OT}$-FLEX-GFP) and subjected to the 3-day contextual fear conditioning paradigm after recovery and handling. Following the first two shock sessions, animals received Dox (5 mg/kg b.w., i.p.) on the 3rd day of the fear conditioning paradigm. On the 4th day, animals were exposed to the fear conditioning chamber, this time without electrical shocks. After the 1st round of fear conditioning in Context A, the animals were transferred to Context B, there they underwent an additional session of fear conditioning in analogy to that in Context A, one week later. All animals were sacrificed 90 min after the beginning of the test session in Context B. This point in time was chosen as it is well established that the c-*fos* protein has its peak expression at around 90 min after the initial activation of OT neurons. To label all neuroendocrine cells protruding beyond the blood brain barrier (most importantly, magnOT neurons), animals received a single injection of Fluorogold, Santa Cruz Biotechnology, Dallas, 15 mg/kg bw i.p. dissolved in 1xPBS, 7 days prior to perfusion (Eliava et al., 2016).

DREADD-based inhibition of parvocellular OT neurons of the PVN in Context B

For this experiment, rats were injected with the retrogradely spreading rAAV-CAV2-Cre into the SON and rAAV-$\mathbf{P}_{OT}$-FLEX-hM4D into the PVN to specifically express hM4D in parvOT neurons of the PVN, in analogy to our previous study (Eliava et al., 2016). After one week of recovery, animals were handled 10 min per day for 1 week. In the 3rd week after injection, animals were subjected to fear conditioning in Context A in analogy to Figure 2A. Following the successful fear conditioning in Context A, animals were transferred to Context B, where another round of fear conditioning was performed (see Figure 4A). Thirty minutes prior to the experiment of day 3 (exposure day), the three experimental animals received an i.p. injection of clozapine-N-oxide CNO (3mg/kg bw i.p., Tocris Bioscience, Bristol, UK, dissolved in 1xPBS) to inhibit the activity of parvOT neurons. The control animals received the same volume of vehicle (0.9% NaCl). Ninety minutes after the start of the session, the animals were euthanized with isoflurane and perfused to collect the brains. Brain sections containing SON were used for immunohistochemical staining for OT and c-*fos*. Quantitative analysis of OT versus c-*fos* expressing cells was performed and the results are demonstrated (in Table S4**)**. Naive animals and animals that were only subjected to Context A served as controls.

Stereotaxic injection of viral vectors and implantation of optic fibers

Injection of viral vectors into the rat brain was performed in analogy to Knobloch et al., 2012. If not indicated otherwise, all hypothalamic nuclei were injected bilaterally using the following coordinates: SON (M-L ± 1.6mm, A-P −1.4mm, D-V −9.0mm), PVN (M-L ± 0.3mm, A-P −1.8mm, D-V −8.0mm) and AN (M-L ± 1.2mm, A-P −2.0mm, D-V −8.5mm). Point of origin for the coordinates was Bregma and the Z level difference of Bregma and Bambda did not exceed 0.1mm (Cetin et al., 2006). Injection volume per injection site was 300 nL (either single virus or cocktail), while all viruses used were in the range of 10^{12} −10^{13} genomic copies per ml. For the implantation of optic fibers into the CeA, we used the following coordinates: M-L ± 3.9, A-P −2.5, D-V −8.0 while the optic fibers had a length of 8.5 mm.

Ex Vivo Electrophysiology

Amygdala

Horizontal slices preparation. Animals were anaesthetized with an intraperitoneally administered mixture ketamine/xylazine (Imalgene 90 mg/kg, Rompun, 10 mg/kg). Transcardial perfusion was then performed using one of the following artificial cerebro-spinal fluids (ACSFs) dissection solutions. For rats between 10 and 11 weeks old, an ice-cold NMDG based ACSF was used containing (in mM): NMDG (93), KCl (2.5), NaH_2PO_4 (1.25), $NaHCO_3$ (30), $MgSO_4$ (10), $CaCl_2$ (0.5), HEPES (20), D-Glucose (25), L-ascorbic acid (5), Thiourea (2), Sodium pyruvate (3), N-acetyl-L-cysteine (10), Kynurenic acid (2). The pH was adjusted to 7.4 using HCl 37%, after bubbling in 95% O_2 and 5% CO_2 gas; bubbling was maintained throughout the duration of use of the various ACSFs. Following decapitation, the brain was swiftly transferred into the same ice-cold ACSFs dissection solution as for transcardial perfusion, and 350 μm thick horizontal slices containing the CeA were obtained using a Leica VT1000s vibratome. After slicing, brain slices were hemidissected and placed in a room-temperature holding chamber with normal ACSF, for a minimum of 1 h before the conduction of any experiments. Slices of 10-11 weeks old rats were placed in 35°C NMDG ACSF for 10 min before transferring them to the holding chamber at room temperature. Normal ACSF, also used during experiments, was composed of (in mM): NaCl (124), KCl (2.5), NaH_2PO_4 (1.25), $NaHCO_3$ (26), $MgSO_4$ (2), $CaCl_2$ (2), D-Glucose (15), adjusted for pH values of 7.4 with HCl 37% and continuously bubbled in 95% O_2 and 5% CO_2 gas. All ACSFs were checked for osmolarity and kept for values between 305-312 mOsm/L. For electrophysiology experiments, slices were transferred from the holding chamber to an immersion recording chamber and superfused at a rate of 2 mL/min with normal ACSF unless indicated otherwise.

CeM Neurons recordings. Pipettes were filled with an intracellular solution containing (in mM): KCl (150), HEPES (10), $MgCl_2$ (4), $CaCl_2$ (0.1), BAPTA (0.1), ATP Na salt (2), GTP Na salt (0.3). pH was adjusted to 7.3 with KOH and osmolality checked to be between 290-295 mOsm/L, adjusted with sucrose if needed. All cells were hold at a membrane potential of −70 mV. Series capacitances and resistances were compensated electronically throughout the experiments using the main amplifier. Average IPSC frequencies were calculated in 20 s windows, chosen for light stimulation at maximal effect, as determined by the maximal slope of the cumulative plot of the number of currents using SigmaPlot 11.0. Baselines and recovery IPSC frequencies were measured at the beginning and end of each recording. Z-score values were calculated by subtracting the average baseline IPSC frequency established over 70 s at the recording beginning from individual raw values and by dividing the difference by the baseline standard deviation. Optical BL illumination of CeL OT axons expressing hChR2 was performed using light source X-Cite® 110LED from Excelitas Technologies through a

GFP filter, controlled with a Clampex-driven TTL pulse for 20 s at 30Hz with 10ms pulses. To quantify the pharmacological blockade (NBQX or dOVT) of the BL illumination on the CeM IPSC frequencies, a ratio was first calculated between basal and BL modified IPSC frequencies minus one and that for each recording neuron, in order to obtain the BL effect. Second, the percentage of the remaining BL illumination after pharmacological blockade was obtained by dividing the BL effect after and before drug perfusion. This is reported as ΔBL/BL0 (%) in Figure 3B2.

SON OT neurons recordings. For this experiment, rats received viral injections of 300 nL vGATE with rAAV-$\mathbf{P}_{OT}$-FLEX-GFP as virus 3 or rAAV-$\mathbf{P}_{OT}$-mCherry bilaterally into the SON. Thus, OT engram cells were labeled in green, while OT non-engram cells in red. Recording pipettes were filled with an intracellular solution containing (in mM): $KMeSO_4$ (125), $CaCl_2$ (2), EGTA (1), HEPES (10), $ATPNa_2$ (2), GTPNa (0.3). pH was adjusted to 7.3 with KOH and osmolality checked to be between 290-295 mOsm/L, adjusted with sucrose if needed. After whole-cell patch-clamp of identified OT neuron, the following parameters were recorded: access resistance, membrane capacitance, resting potential, spontaneous EPSC amplitude and frequency, response to current injection (0 to 150 pA for 500ms, with steps of 25 pA).

Optical stimulations. Optical BL illumination of CeL OT-ergic axons expressing hChR2 was performed using light source X-Cite® 110LED from Excelitas Technologies through a GFP filter, controlled with a Clampex-driven TTL pulse for 20 s at 30Hz with 10ms pulses.

Analysis of effect of blue light. Average IPSC frequencies were calculated in 20 s windows, chosen for light stimulation at maximal effect, as determined by the maximal slope of the cumulative plot of the number of currents using SigmaPlot 11.0. Baselines and recovery IPSC frequencies were measured at the beginning and end of each recording. Z-score values were calculated by subtracting the average baseline IPSC frequency established over 70 s at the recording beginning from individual raw values and by dividing the difference by the baseline standard deviation.

Pharmacological assays. To quantify the pharmacological blockade (NBQX or dOVT) of the BL illumination on the CeM IPSC frequencies, a ratio was first calculated between basal and BL modified IPSC frequencies minus one and that for each recording neuron, in order to obtain the BL effect. Second, the percentage of the remaining BL illumination after pharmacological blockade was obtained by dividing the BL effect after and before drug perfusion. This is reported as ΔBL/BL0 (%) in Figure 3B2.

Histology

Animals were perfused through the heart with 1x PBS, followed by 4% paraformaldehyde to fixate the tissue and extracted brains were post-fixed overnight.

The hypothalamus

Brain sections (50 μm) were collected by vibratome slicing and immunohistochemistry was performed with the following antibodies: chicken anti-GFP (Abcam; 1:10000), anti-OT (PS38, 1:1000; mouse; kindly provided by Harold Gainer); anti-c-*fos* (1:1000; rabbit; Santa Cruz Biotechnology), anti-Fluorogold (1:1000, guinea pig, Protos Biotech) and anti-DsRed (1:1000; rabbit; Clontech). GFP signal was enhanced by FITC-conjugated IgGs, hChR2-mCherry signals by CY3-conjugated antibodies and, for different experiments, other markers were visualized by FITC-conjugated; CY3-conjugated or CY5-conjugated antibodies (1:500; Jackson Immuno-Research Laboratories). Nuclei of cells were visualized with DAPI (1:1000; Roche). All images were acquired on a confocal Leica TCS SP5 and Zeiss LSM5 microscopes; digitized images were analyzed using Adobe Photoshop. To quantify vGATE-assisted labeling of cells, we counted all OT-, hChR2-immunoreactive neurons in the SON and PVN (8-150 neurons/section dependent on the anterior-posterior Bregma level) in 5 animals (3 sections for SON and PVN) with the stereotactic rostro-caudal Bregma coordinates (PVN: −1.5, −1.8, and −2.0 mm; SON: −1.1, −1.4, and −1.7 mm). Statistical significance was determined by Student's test for colocalization experiments, OT axon morphology and statistical analysis was performed with Prism 5 (Mac OS X). Results are presented as mean ± SEM.

The amygdala

Staining for the vesicular glutamate transporter vGluT2. Selected sections containing the CeA were then immunolabeled for darkfield and brightfield microscopy. For darkfield fluorescent staining, the cocktail containing different combinations of primary antibodies: anti-vGluT2 (1:2000; rabbit; SySy), anti-OT (1:2000, mouse), anti-DsRed (1:1000; rabbit; Clontech), anti-GFP (1:10,000, chicken, Abcam) were used. The named antigens were detected using appropriate secondary antibodies conjugated with fluorophores of various excitation ranges (Alexa488, Alexa459, Alexa680, Thermofisher). All tissue samples, labeled with fluorescent markers were imaged using Leica SP5 CLSM, and digitized using Adobe Photoshop software. To evaluate the CeL vGluT2 expression level, we processed the tissue for triple GFP, OT and vGluT2 immunolabeling in rats of $OT^{Constitutive}$ and OT^{vGATE} groups. In total, 2000 varicosities per animal group were counted and visually examined to detect the presence of double GFP-vGluT2 signals. The final numbers were computed as a proportion (percentage). For brightfield immunostainings, secondary antibodies conjugated to biotin were used. Final visualization of labeling was carried out with standard ABC HRP Kit (Vector) using DAB as a chromogene. The bright microscopic images were captured using a Nikon Eclipse microscope E200 (Software: Nikon NIS-Elements Version 4.30). We analyzed the number of varicosities and the mean length of OT fiber segments residing in the CeL to trace possible structural changes. Altogether, 72 coronal planes of 6 rats in the OT^{vGATE} group (and 7 in control) were used for this type of analysis. Length of GFP-positive fibers and number of axonal varicosities were measured and counted using free hand tracing and touch-count options in the latest version of ImageJ software (NIH). All statistics were processed in group-specific comparisons between two groups (t-Test, $p < 0,05$, one-tailed), always in one and the same plane of CeL (Bregma: −2,4 to −2,8).

Staining for Somatostatin, Corticotropin-Releasing-Hormone and c-fos. For triple labeling of c-Fos, (Abcam, 1: 1 000), CRH (Peninsula Labs., 1: 10 000), and SOM (Chemicon, 1:500), combination of DAB technique (c-Fos detection) and fluorescent labeling (for CRH and SOM) was applied. First, the sections were incubated with c-Fos antibody and developed using biotinylated secondary antibody, ABC kit (Vector) and conventional DAB detection protocol. Second, the c-Fos DAB-developed tissue was processed for anti-gene retrieval procedure via "boiling" sections in Tris Buffer Saline pH10 at 95°C for 1h for optimal detection of CRH and SOM in the somas of CeA neurons. Afterward all primary and secondary labeling steps for CRF and SOM detection were performed as described. The actual figures represent digital overlays of confocal bright-field scans of DAB-detected c-Fos and florescent-labeled CRH and SOM. All images were obtained using Leica SP5 CLSM (Imaging Facility, DKFZ, Heidelberg).

Fluorogold treatment and visualization. To discriminate between magno- and parvocellular OT neurons, animals received a single injection of Fluorogold (Santa Cruz Biotechnology, Dallas, 15 mg/kg bw i.p.) 7 days prior to the perfusion. Brain sections were stained with a primary antibody for Fluorogold (Guinea pig anti-FG, dilution 1:1000, Protos Biotech Corp, New York) and Fluorogold immunosignal was visualized by secondary antibodies conjugated with CY3 (Donkey anti-rabbit, dilution 1:500, Jackson Immuno Research, Newmarket Suffolk, UK) or Alexa 680 (Alexa 680: Goat anti-guinea-pig, 1:1000, ThermoFisher Scientific, Waltham, Massachusetts). The colocalization of Fluorogold, OT (or c-*fos*) and GFP signals was quantified in the PVN (SON contains only magnOT neurons), (n = 10; 4 sections/brain). Quantitative analyses of parvo- and magnocelluar OT cells expressing GFP are presented in Table S6.

Retrobeads infusion. For the retrograde labeling of vGATE projections terminating in the CeA we used retrobeads from LumaFluor. We used the following coordinates for infusion in accordance with Bregma: (CeA left/right): ML: ± 4.0 mm, AP: 2.5 mm and DV: −8 mm, without angle and an injection volume of 140 nl.

Cannula implantation. Animals were bilaterally implanted with guide cannulas for direct intra-central lateral amygdala infusions. We used the C313G/Spc guide metallic cannulae (Plastics one, VA, USA) cut 5.8 mm below the pedestal. For this purpose, animals were deeply anesthetized with 5% isoflurane and their heads were fixed in a stereotaxic fame. The skull was exposed and two holes were drilled according to coordinates that were adapted from a rat brain atlas (2.3 mm rostro-caudal; 4 mm lateral; 7.5 mm dorso-ventral relative to bregma) by comparing the typical bregma-lambda distance (9 mm) with the one measured in the experimental animal. Two screws were fixed to the caudal part of the skull in order to have an anchor point for the dental cement. Acrylic dental cement was finally used to fix the cannula and the skin was sutured. CNO infusion (1 μm) occurred at 20 nl/s with a final infusion volume of 100nl per CeA.

Measurement of Plasma ot Concentrations

Plasma preparation for LC-MS/MS analysis

50 pmol of D5-oxytocin internal standard was added to 200 μl of lithium heparin plasma. Plasma was acidified with an equal volume of 5% H_3PO_4 (v/v) and was centrifuged (14,000 x g, 5min). The resulting supernatants were collected and adjusted to 1% H_3PO_4 with H_2O prior to solid phase extraction (SPE). The SPE procedure was performed with a positive pressure manifold (Thermo Electron). OASIS HLB SPE-cartridges (1cc, 30mg, Waters, Guyancourt France) were first activated with 1ml of acetonitrile (ACN) and then washed with 1ml of H_2O 99% / H_3PO_4 1% (v/v). The sample was loaded and the SPE-cartridge and the cartridge was washed with 1ml of H_2O 99% / H_3PO_4 1%. After a 1ml wash with H_2O/formic acid 0.1% (v/v) and with 1 mL of ACN 5% / H_2O 94.1% / formic acid 0.1% (v/v/v), elution was performed with 500 μl of acetonitrile 60% / H_2O 40% (v/v). Eluates were collected and dried under vacuum prior to MS analysis (see below).

LC-MS/MS instrumentation and analytical conditions

LC-analyses were used to determine the presence of oxytocin in the selected reaction monitoring mode (SRM). Analyses were performed on a Dionex Ultimate 3000 HPLC system (Thermo Scientific, San Jose, CA, USA) coupled with a triple quadrupole Endura (Thermo Scientific). The system was controlled by Xcalibur v. 2.0 software (Thermo Scientific). Extracted plasma samples were solubilized in 100 μl of H_2O/formic acid 0.1% (v/v) and 20 μl of the solution were loaded into an Accucore RP-MS column (ref 17626-102130; 100 × 2.1 mm 2.6 μm, Thermo Electron) heated at 35°C. Oxytocin and D5-oxytocin elutions were performed by applying a linear gradient of buffers A/B. Buffer A corresponded to H_2O 98.9% / formic acid 0.1% (v/v), whereas buffer B was ACN 99.9%/ formic acid 0.1% (v/v). A linear gradient of 20%–95% of solvent B at 400 μL/min over 2.5min was applied followed by a washing step (0.5min at 95% of solvent B) and an equilibration step (1min of 20% of buffer B). Qualitative analysis and quantification were performed in SRM using an Endura triple quadrupole mass spectrometer and deuterated internal standards. For ionization (positive mode), 3500V of liquid junction voltage and 350°C capillary temperature was applied. The selectivity for both Q1 and Q3 was set to 0.7Da (FWHM). The collision gas pressure of Q2 was set at 2mTorr of argon. For oxytocin and D5-oxytocin, the selection of the monitored transitions and the optimization of the collision energy were preliminarily and manually determined. The transitions and the corresponding collision energies (CE) used for SRM were the following: m/z 504.2 → m/z 285.1 (CE = 15.9 eV), m/z 504.2 → m/z 487.2 (CE = 11.9 eV) and m/z 504.2 → m/z 495.7 (CE = 10.2 eV) for oxytocin with 2 charges; m/z 506.8 → m/z 290.2 (CE = 16.2 eV), m/z 506.8 → m/z 492.9 (CE = 12.9 eV) and m/z 506.8 → m/z 498.3 (CE = 10.7 eV) for D5-oxytocin (with 2 charges). Identification of the compounds was based on precursor ion, selective fragment ions and retention times obtained for oxytocin and D5-oxytocin internal standard. Quantification of oxytocin was done using the ratio of daughter ion response areas of the D5-oxytocin.

Measuring of signal intensity via Fiji (ImageJ)

To compare the signal intensity of neurons or axonal terminals we used the Image Intensity Processing function of ImageJ. Following the detailed description of the analysis (https://imagej.net/Image_Intensity_Processing), we converted the .lif files from the confocal microscope into TIFF images and opened them with ImageJ. For the signal intensity analysis, we used the raw data with no contrast modifications or gamma corrections. The freehand tool was used to delineate the axonal segments and the average signal intensity of the region of interest (ROI) was calculated via the 'Analyze-Measure' function. For the analysis of signal intensity in axons, the entire length per section was used for the quantifications. The numeric values presented in the manuscript represent the output values of ImageJ obtained from the signal intensity measurements. To specifically identify OT-positive varicosities, we first calculated the average signal intensity (via 'Measure-Analyze') and standard deviation of all images included in the data analysis. Next, we used the freehand tool / line to delineate the ROI of the axonal segments and measured the signal intensity. We defined an axon to be 'OT-positive', if the signal intensity within the ROI exceeded the average signal intensity of the included images by at least 4-times the standard deviation. Axonal terminals that could not fulfill this criterion, were considered OT-negative.

QUANTIFICATION AND STATISTICAL ANALYSIS

Quantitative analysis (cell counting, c-*fos* expression and axon length) was performed in a double-blind manner using Fiji or Adobe Photoshop and a superimposed grid feature. Statistical analysis was performed using GraphPad Prism 7. $p < 0.05$ was considered as statistically significant (Tables S1–S6).